

EXPERIMENTAL TESTS OF THE STANDARD MODEL

L. NODULMAN
Argonne National Laboratory
High Energy Physics Division
Argonne IL 60439 USA

1. Introduction

The title implies an impossibly broad field, as the Standard Model includes the fermion matter states, as well as the forces and fields of $SU(3) \times SU(2) \times U(1)$. For practical purposes, I will confine myself to electroweak unification, as discussed in the lectures of M. Herrero. Quarks and mixing were discussed in the lectures of R. Aleksan, and leptons and mixing were discussed in the lectures of K. Nakamura. I will essentially assume universality, that is flavor independence, rather than discussing tests of it.

I will not pursue tests of QED beyond noting the consistency and precision of measurements of α_{EM} in various processes including the Lamb shift, the anomalous magnetic moment ($g-2$) of the electron, and the quantum Hall effect. The fantastic precision and agreement of these predictions and measurements is something that convinces people that there may be something to this science enterprise.

Also impressive is the success of the “Universal Fermi Interaction” description of beta decay processes, or in more modern parlance, weak charged current interactions. With one coupling constant G_F , most precisely determined in muon decay, a huge number of nuclear instabilities are described. The slightly slow rate for neutron beta decay was one of the initial pieces of evidence for Cabibbo mixing, now generalized so that all charged current decays of any flavor are covered.

QCD has also evolved an impressive ability to predict a wide range of measurements with a universal coupling, α_S . Tests of QCD were covered in the lectures of J. Stirling. Clearly the issues of associating final state jets with quarks and gluons, and of analyzing proton structure in terms of quarks and gluons will be important in many experimental tests of electroweak unification.

The lack of renormalizability of the Fermi theory of charge current weak interactions, that is the inability to calculate radiative corrections, and thus bad behavior in the high energy limit, was the motivation for models of unification. One of several such models, which, in the early 70's went under the name "Weinberg-Salam," [1] has become "Standard." A simple-minded picture of this model is that by combining an isosinglet and a isotriplet of gauge bosons, one mixes up the γ for QED, heavy W^\pm bosons for the weak charged current, and a heavy Z^0 which predicted the weak neutral current interaction. A third parameter describing the neutral weak interaction can be taken as some definition of the weak neutral triplet/singlet mixing angle, Θ_W , or more practically, as the rather precisely measured mass of the Z^0 boson. A fourth parameter is needed, associated with consistency in heavy gauge boson masses; this may be taken as the Standard Model Higgs mass, which is largely decoupled from observables.

For practical purposes, I will consider the Standard Model to include the simplest Higgs mechanism, one complex doublet, with one residual Higgs particle with a mostly unpredicted mass. Implementation of the Higgs mechanism in terms of fundamental scalar multiplets may well be just a mathematical trick; one certainly hopes that nature could not really be so unimaginative. But since the simplest scheme is still viable, I will take it as standard. I note that in terms of multiple Higgs states, infinite variety is possible, although there are some constraints from measurements of the ρ parameter, as M. Herrero discussed in terms of "custodial symmetry."

The unified electroweak theory does allow calculation of radiative corrections. These corrections give terms involving squares of fermion masses, and logarithms of scalar masses, for example, in predicting the weak mixing angle and/or the W boson mass. That is, heavier masses imply larger effects. These would include particles we may not know about, as well as particles regarded as standard. So if everything hangs together in terms of the top quark mass and the Higgs mass, we obtain constraints on what else could be out there.

Precision measurements to challenge these predictions have been an essential feature of e^+e^- collider studies culminating in the LEP and SLC programs. The predictions serve as a motivator for high energy hadron collider programs, from the $S\bar{p}pS$ collider at CERN, to the current Fermilab Tevatron Collider, and the LHC being built at CERN. Most processes involve "oblique" or propagator corrections; these involve top mass squared and Higgs mass logarithmic terms. Notably the Z^0 decay rate to b pairs, R_b , depends on vertex corrections which depend essentially on the top mass. One of the claims of success of this precision measurement program has been the consistency of the indirectly implied top mass with the hadron collider top mass limits and, eventually, top mass measurements. Thus, the

measurement of the top mass is an essential part of the program, which has moved on to constraining the Higgs.

I will review several measurements to illustrate this program: The new muon (g-2) experiment at Brookhaven illustrates both weak and QED measurement. The NuTeV experiment at Fermilab illustrates the historically important and currently still competitive contribution of neutrino physics. The LEP precision Z^0 lineshape and Z^0 decay asymmetry measurements are clearly the core of this program. The ultimate Z^0 asymmetry measurement comes, of course, from SLC. The increasingly precise W boson mass measurements at the Tevatron have been joined by measurements at LEP2. The top mass measurements complete the indirect Higgs picture, but the direct Higgs search at LEP2 has a significant impact as well.

2. BNL E815 MUON (g-2)

2.1. GOALS OF THE MEASUREMENT

The anomalous magnetic moment of the muon, defined as

$$a_\mu \equiv \mu_\mu / (e\hbar/2m_\mu) - 1 = (g_\mu - 2)/2,$$

is a less favorable QED test than the electron magnetic moment. The heavier muon mass makes radiative corrections involving hadronic states relatively important. The heavier muon mass also makes electroweak radiative corrections relatively important. Previous measurements at CERN[2] were precise enough to establish the presence of hadronic corrections. The goal at Brookhaven is to measure a_μ well enough to get a handle on the electroweak radiative corrections; a requirement for this is a precise enough prediction of hadronic corrections to allow the EWK corrections to be isolated.[3]

TABLE 1. Values and corrections to a_μ in units of 10^{-11} .

Quantity	Value	Error
QED prediction	116584706	2
EWK correction	151	4
HAD correction	6771	77
Overall prediction	116591628	77
CERN measurement	116592300	840

The magnetic moment numbers are given in Table 1. The QED prediction is calculated to α^5 [4] and the EWK correction is calculated to two

BNL MUON G-2 EXPERIMENT

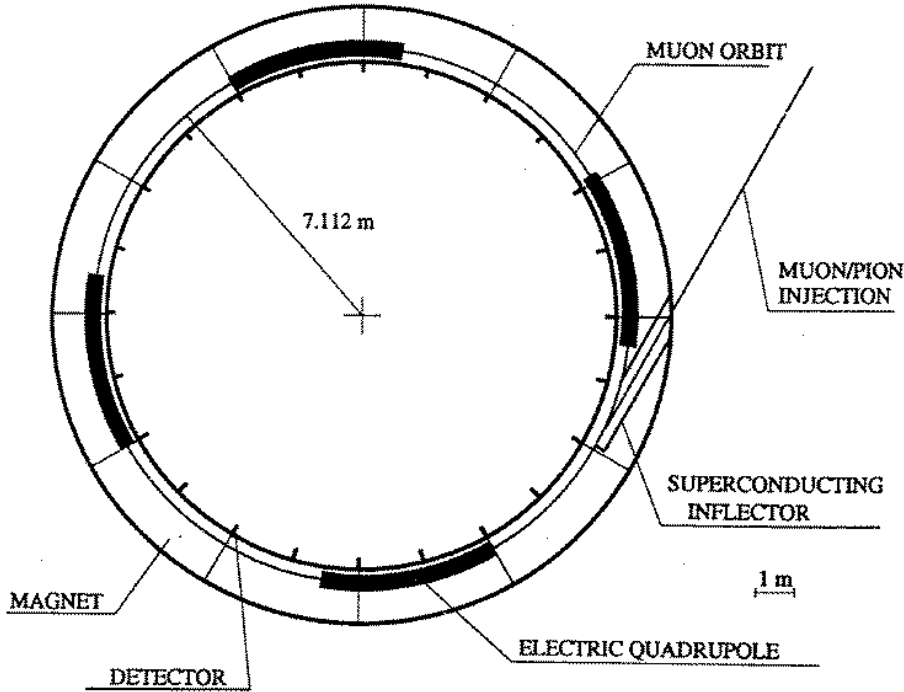


Figure 1. The Brookhaven g-2 muon storage ring.

loops.[4, 5] The leading order hadronic correction, a vacuum polarization loop with hadrons, must be determined with dispersion relations, using the low energy $e^+e^- \rightarrow \text{hadrons}$ measurements.[6] These measurements are being improved at CMD2 in Novosibirsk, BES, and in τ decay studies. Higher order hadronic corrections, and light-by-light or diagrams with four photons converging on a loop[7] are relatively under control.

While it is clear that the current level of prediction creates a market for improving on the CERN measurement, the predicted level of EWK corrections at 151×10^{-11} is not all that much bigger than the error of 77×10^{-11} in the prediction, which is dominated by the hadronic uncertainty. Improving the low energy e^+e^- measurements is a clear concurrent goal. The Brookhaven goal for measurement precision is $\pm 35 \times 10^{-11}$ for both μ^+ and μ^- .

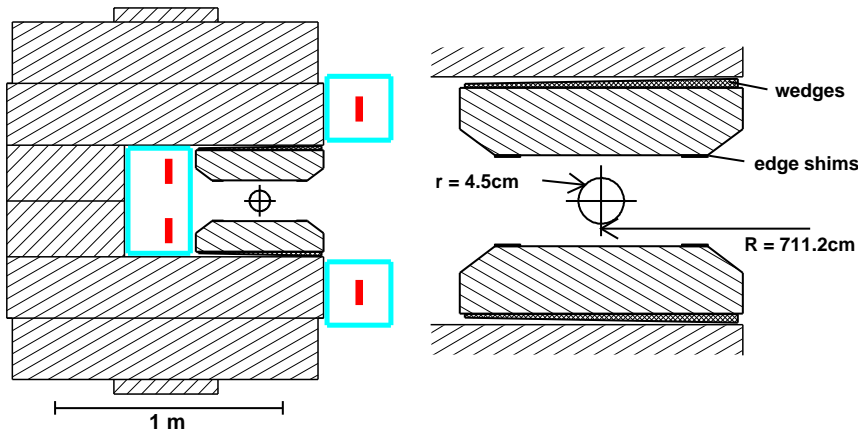


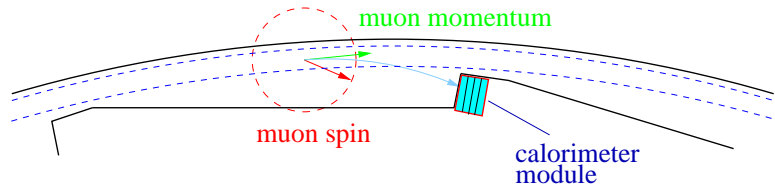
Figure 2. The profile of the g-2 muon storage ring magnet. The boxes are the vessels for superconducting cable. The detail on the right shows allowance for field adjustment.

2.2. METHOD OF MEASUREMENT

The charged pion decays by the weak charged current to $e\bar{\nu}_e$ or $\mu\bar{\nu}_\mu$. The V-A form implies that the zero (or negligible) mass of the neutrino forces helicity selection. To conserve angular momentum in the decay of the zero spin pion, the massive charged lepton must be in the helicity state disfavored by V-A. Since the muon is much heavier than the electron, the electron channel is much more suppressed by helicity, $\sim 10^{-4}$. The muons are longitudinally polarized. So if you have a beam of pions, muons from forward decay have the least momentum change and will most likely remain in the beam. Thus, one can readily obtain beams of longitudinally polarized muons. The basic method of the experiment is to put polarized muons in a magnetic field and measure their spin precession. The highest momentum electrons in the decay $\mu \rightarrow e\bar{\nu}_e\nu_\mu$ analyze the muon spin.

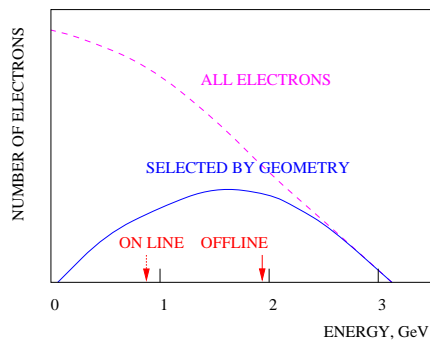
The experiment is done by putting muons into a storage ring. Lots of physics results come from various storage rings, but the g-2 ring, shown in Fig. 1, is rather different. For a precision measurement, you need as well known and as uniform a magnetic field as possible. Thus, the ring is a continuous bending magnet. The injection needs to be carefully done to avoid messing that up. The time scale for storage is short due to the muon lifetime, so imbedded electrostatic quadrupoles are sufficient to capture the beam. Decay electrons are detected in stations at the array of windows.

Gedanken Problem. The g-2 ring uses an iron dominated superconducting magnet, which would not be much stronger than typical conventional storage ring bending magnets. The design momentum is 3.1 GeV/c. The



Shape of the ring vacuum chamber is designed to optimize the decay electron detection.

ELECTRON ENERGY SPECTRA



High energy electrons provide most information about spin rotation signal.

Figure 3. Top: the decay electron window in the vacuum. Bottom: the energy spectrum of detectable electrons with online and offline thresholds marked.

SPEAR storage ring at SLAC, original home of Ψ_s , χ_s , D_s , τ_s etc., has a design momentum of 4 GeV/c, yet it is something like five times larger than the g-2 ring. Why?

Injection is clearly an important problem. So far, they have used pion decay. at the appropriate fortunate time, to give a slight momentum kick for injection. This is rather inefficient, and the pions which do not decay run into things, creating a blast of stuff in the detectors, so that measurements must wait till the detectors are stable. A fast kicker is in the works so that a muon beam can be directly injected.

Magnet quality is an ongoing project. The ring magnet profile is shown in Fig. 2. Field mapping and orbit studies feed back to shimming the iron pole tips. The profile and absolute value are both important; an NMR

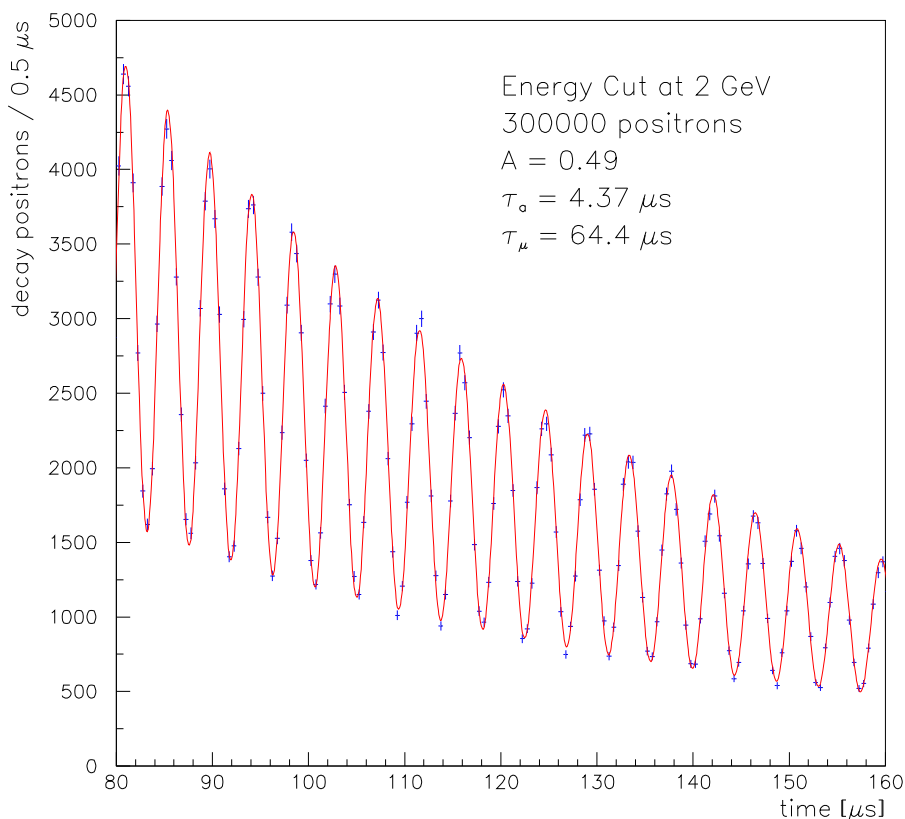


Figure 4. The time spectrum of detected electrons. The period gives a_μ . They may eventually improve G_F .

probe provides the absolute field value by reference to the proton magnetic moment.

Gedanken Problem. The iron dominated superconducting magnet provides good opportunity to control field quality. For the beyond LHC generation hadron collider, VLHC or Eloiseatron, what are the tradeoffs between high field (coil dominated) and iron dominated bending magnets?

What you want to measure is the difference in the cyclotron frequency and the spin precession frequency given by

$$\omega_a = \frac{e}{mc} [a_\mu B - (a_\mu - 1/(\gamma^2 - 1))(B \times E)].$$

At Brookhaven, as at CERN, they choose the “magic gamma” for momentum of 3.09 GeV/c, so the measurement is not sensitive to the electrostatic quadrupole field.

The experimental measurement is illustrated in Fig. 3. The decay electron exits a window on the inside of the ring, and is detected with timing and energy in scintillating fiber calorimeters. The highest energy electrons are most correlated to spin direction. Thus, understanding the selection threshold imposes constraints on calibration and the stability of the calorimeter.

Gedanken Problem. Consider the general cases, as described in J. Virdee’s lectures, of calibration systems for calorimeters contrasting setup for data taking and *in situ* maintenance.

2.3. RESULTS AND PROSPECTS

The measurement is illustrated in Fig. 4, measuring[8]

$$a_{\mu^+} = 116592500(1500) \times 10^{-11}.$$

The level of the statistical error is approaching CERN. The systematics are at the level of $\sim \pm 300 \times 10^{-11}$, including magnetic field systematics and detector related uncertainty.

Work is going into various improvements. Muon injection will give a big statistical boost. Field improvements with shims and trim coils will improve systematics, as will improved detector understanding and tracking of the electrons to verify where the muon beam is. And, of course, the hadronic correction prediction is also getting attention.

In 1998, they expect to get to the level of $\pm 115 \times 10^{-11}$ for μ^+ . Full design precision for both muon charges should be realized in 2002.

3. NuTeV

3.1. GOALS OF THE MEASUREMENT

NuTeV is the latest incarnation of the CCFR (Chicago, Columbia, Fermilab, Rochester) neutrino experiment at Fermilab. They were off looking for wrong-sign heavy leptons when Gargamelle observed neutral currents. Their confirmation of neutral currents at the 1974 London Rochester conference silenced the many vocal skeptics, thus contributing to the recognition of electroweak unification.

The basic measurement then and now is to measure the relative rate of neutral current (NC) and charged current (CC) interactions, measuring

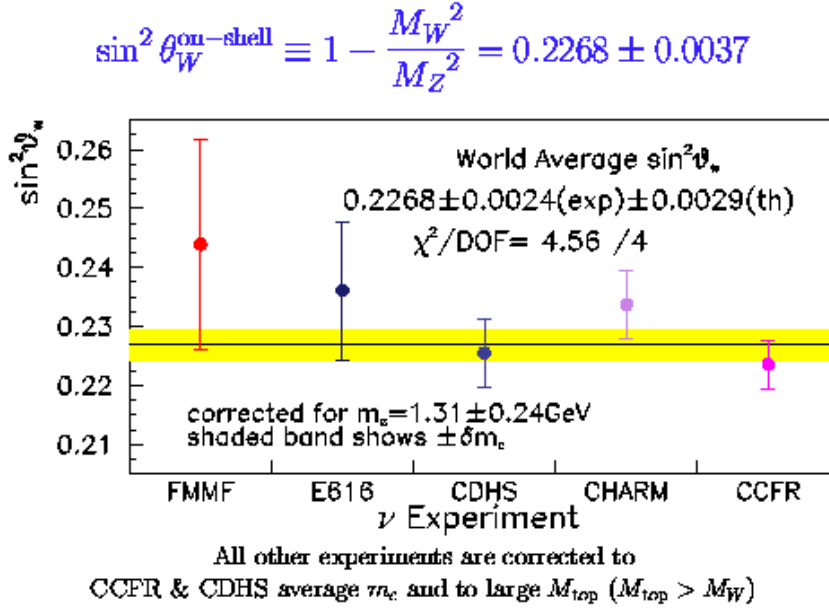


Figure 5. The evolution of neutrino weak mixing measurements showing the charm systematic limit.

the on-shell weak mixing angle

$$\sin^2 \Theta_W^{on-shell} \equiv 1 - \frac{m(W)^2}{m(Z)^2}.$$

The experiment uses muon neutrinos and distinguishes NC from CC by the absence of penetrating muons in the final state. Over several generations of such experiments, systematics such as detailed understanding of the boundaries of the detectors, and more importantly, the charm quark mass, have limited the measurement, as seen in Fig. 5. Neutrinos can interact with a strange sea quark, producing charm; the charm decay can give a muon, complicating the measurement. The charm mass is needed to predict the CC rate. Two muon events can be used to get some measure, but this seems to have plateaued at the level, in the appropriate QCD order, of $m_c \sim 1.3 \pm 0.3 \text{ GeV}/c^2$. Another important systematic effect is the level and understanding of ν_e in the beam, as electron CC look like muon NC. Electron neutrinos from decays of K_L^0 from the production target are a problem due to significant uncertainties in the K_L^0 production rate.

The basic goal of the NuTeV measurement is to escape these systematic limits. By creating a beam with very little neutrino/antineutrino cross talk, it can use the Paschos-Wolfenstein relation[9]

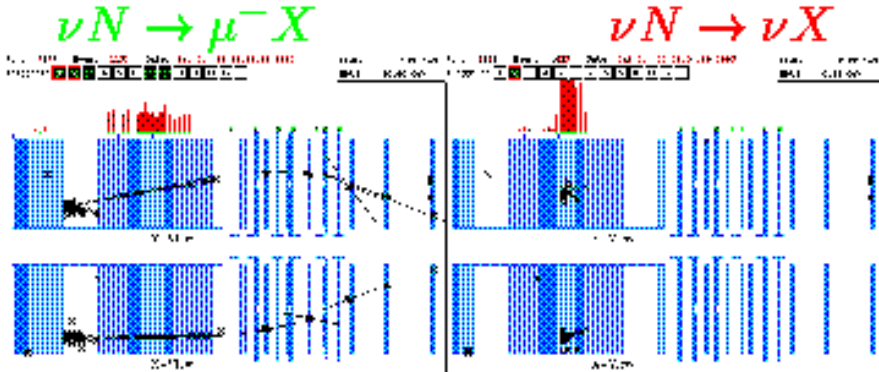


Figure 6. Neutrino interactions in NuTeV/CCFR, left CC and right NC.

$$(\sigma_{NC} - \sigma_{\bar{N}C})/(\sigma_{CC} - \sigma_{\bar{C}C}) = \rho^2(1/2 - \sin^2\Theta_W),$$

obtaining weak mixing from the difference of neutrino and antineutrino cross sections. Thus, the sea cancels and the remaining difference in charm production, due to valence d quark, is Cabibbo suppressed. The goal is to make a competitive inference of the W mass.

3.2. METHOD OF MEASUREMENT

The CCFR detector consists of 690 tons of tracking calorimeter with transverse square planes of iron, liquid scintillator, and drift chambers. The central 390 tons are considered fiducial. This is followed by an extensive system of drift chambers and iron toroids to measure muon momentum. The basic measurements are illustrated with event pictures, see Fig. 6.

The most significant change for NuTeV, compared to CCFR, is the beam. Neutrino experiments typically use zero degree production to optimize yield, using magnetic horn focusing for broad-band beams, or beam line (quadrupole) focusing for narrow-band beams. The NuTeV beam, shown in Fig. 7, looks away from zero degrees, avoiding sensitivity to upstream scraping, reducing the contribution from K_L^0 decays, and thoroughly removing wrong sign particles. The usual decay region is followed by muon shielding, then the detector. Thus the beam should be well understood, as is illustrated in Fig. 8. Note the two peaks corresponding, left-to-right, to neutrinos from pion and kaon decays. Residual beam systematics are dominated by the $K^\pm \rightarrow e3$ branching ratio uncertainty. The flux can be studied with quasielastic CC events, $\nu p \rightarrow \mu n$ with perhaps nuclear breakup, but not pion production.

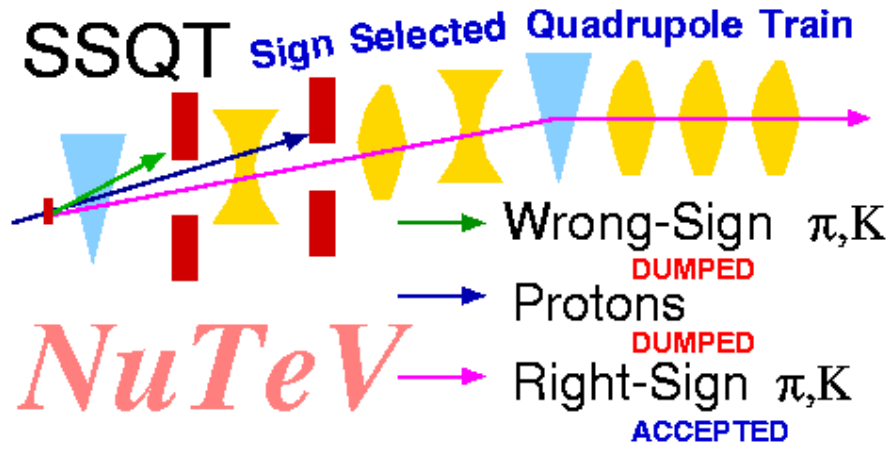


Figure 7. NuTeV production target and beam line into the decay region.

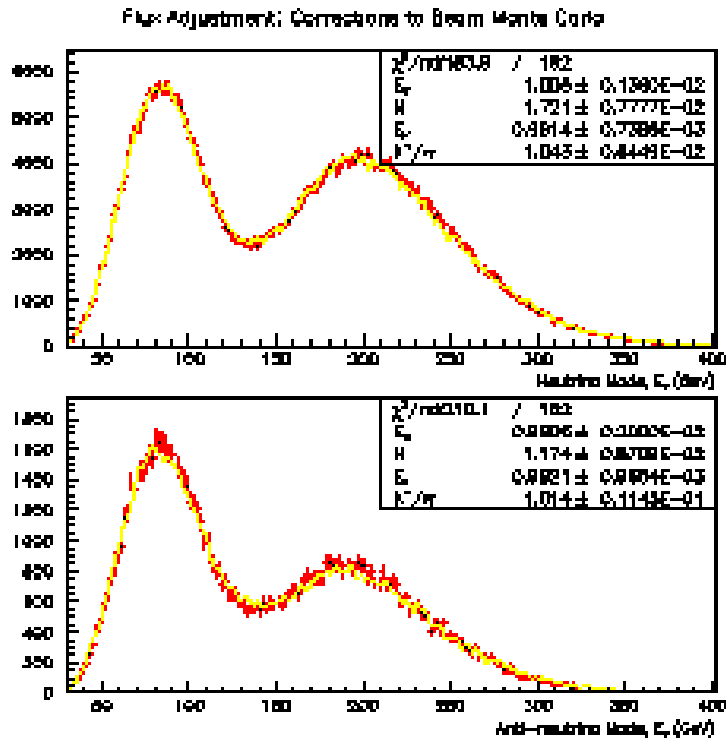


Figure 8. NuTeV neutrino and antineutrino flux, detected and MC.

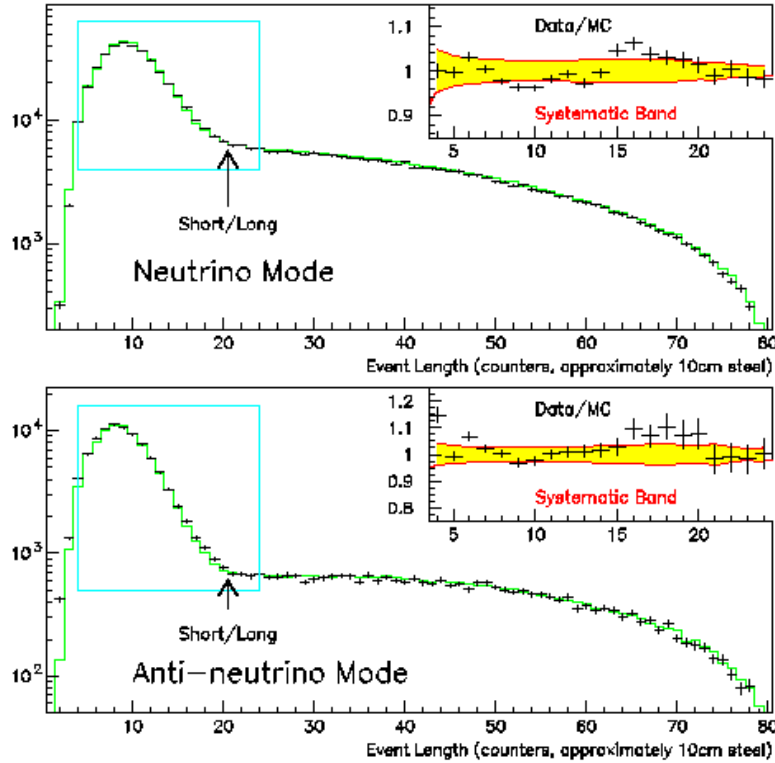


Figure 9. NuTeV neutrino and antineutrino events as a function of event length. Insets are data/MC ratios in the region of the cut.

Gedanken Problem. Consider the general problem of high intensity production targeting - how would you optimize for producing antiprotons, muons, or tau neutrinos?

The basic measurement consists of measuring the length of events. Length is measured in units of counter planes, which are separated by 10 cm of iron. The boundary between short and long is taken at 20 planes. A concurrent test beam line allows the detector, including boundaries where muons could sneak out, to be well understood. Convolving this understanding with the flux in Monte Carlo simulation should allow a detailed understanding of length distributions as illustrated in Fig. 9. The region of the cut is reasonably well described, as shown in the insets, and the ratio short/long can be unfolded to give NC/CC.

3.3. RESULTS AND PROSPECTS

The NuTeV run was completed in 1997, and preliminary results have been given.[10] The statistical precision for $\sin^2\Theta_W$ is ± 0.00190 , comparable to the CCFR result. The physics model systematics level is ± 0.00070 , with detector systematics at ± 0.00075 . Unlike CCFR, the NuTeV measurement is statistically dominated. Using the measured top mass, the NC/CC ratio gives $\sin^2\Theta_W = 0.2253 \pm 0.0022$, which corresponds to $m(W) = 80.26 \pm 0.11$ GeV/c². Combining NuTeV with the CCFR result gives

$$\sin^2\Theta_W^{on-shell} = 0.2255 \pm 0.0021.$$

Their goals have been largely achieved. Some improvement in experimental systematics may come with further analysis. No further data taking is planned.

4. Digression on Collider Detectors

The experiments remaining are at either e^+e^- or $\bar{p}p$ colliders. Almost all such collider detectors, as well as those at HERA, are quite similar. Good examples, ATLAS and CMS for LHC, were thoroughly described in the lectures of F. Pauss. A tracking volume around the interaction is defined inside a solenoid. These days drift chambers for magnetic tracking are complemented, as discussed in the lectures of I. Abt, by silicon detectors. There may also be particle ID. The tracking volume is surrounded by calorimeters, and a muon identification system surrounds that. This is illustrated by SLD, shown in Fig. 10.

Electrons are identified by matching a track to suitable calorimeter measurements. Muons match a track inside to a track or track stub outside. To identify τ leptons, one demands one or three tracks corresponding to a relatively narrow calorimeter energy cluster, isolated from other activity. In the case of hadron colliders, the detectors must make ID information available for fast triggers.

The silicon detectors are used to identify b quarks by observing secondary vertices. This procedure is usually marginal for charm, and c quarks tend to be identified by reconstructing exclusive D decay modes or using the soft pion from $D^* \rightarrow \pi^\pm D$ with partial reconstruction of the D to show the low Q for the pion. Clearly, b and c identification are correlated; charm decay is only three times faster, and bottom decays produces charm.

Gedanken Problem. How would you trigger, at a hadron collider, on τ leptons? Has this worked?

The first detector of this form was Mark I at SPEAR in the early 70s. CDF at the Tevatron was the first such for hadron colliders. Notable ex-

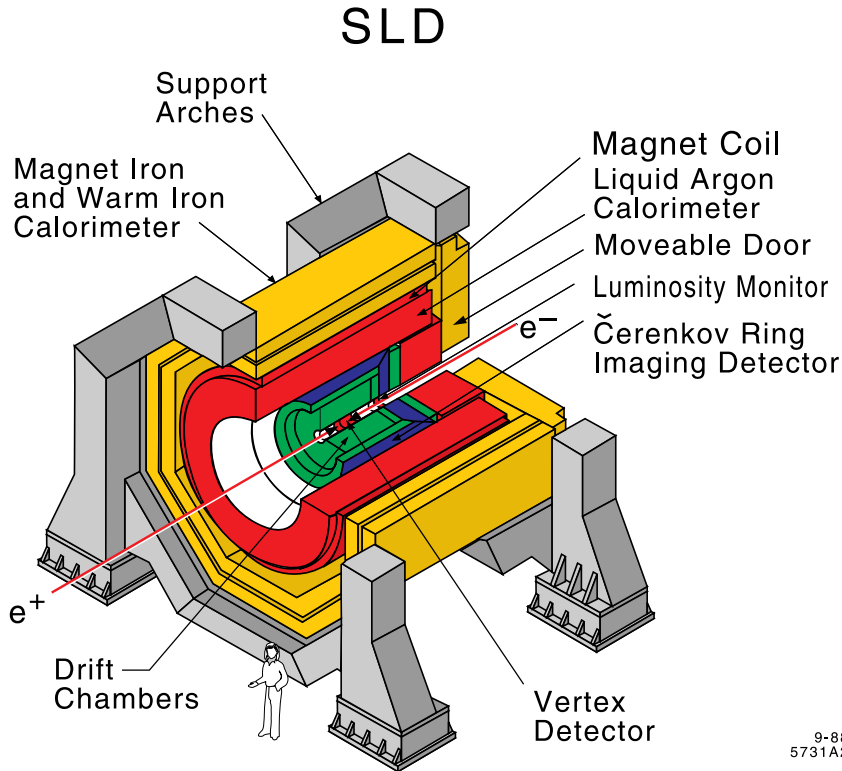


Figure 10. SLD as an example of a generic collider detector. The warm iron calorimeter doubles as a muon detector.

ceptions with no central field are the Crystal Ball, UA2, and pre-upgrade DØ. UA1 had a dipole magnet.

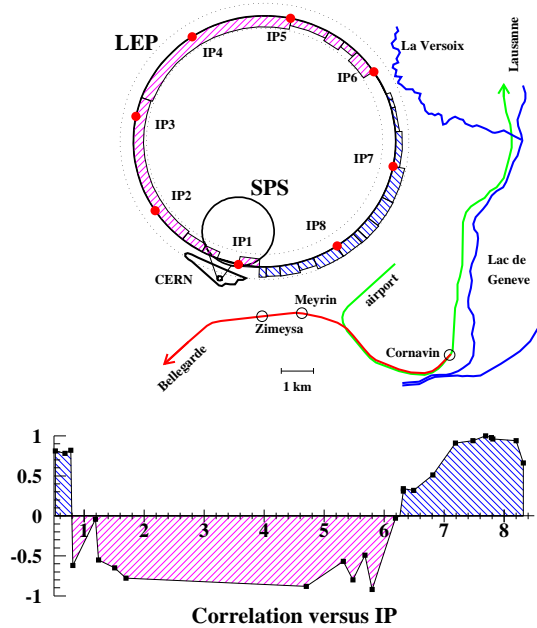
5. LEP1 Z Studies

5.1. GOALS OF THE MEASUREMENT

The basic goal of the LEP1 program was a comprehensive study of the Z boson. The Z is observed as an s channel resonance in e^+e^- collisions. The important issues here are the Z lineshape, basic aspects of decays, and in particular the charge and τ polarization asymmetries which result from parity violation. The presence of both vector and axial vector coupling gives asymmetries which measure weak mixing. A definition of the weak mixing angle $\sin^2\Theta_{W_{eff}}$ is used which avoids loss of precision to uncertain top and Higgs mass dependence. For leptons, this is simply

$$\sin^2\Theta_{eff}^{lept} \equiv 1/4(1 - g_{V\ell}/g_{A\ell}).$$

Vacuum Chamber Current Correlation



B. Dehning, M. Geitz

Figure 11. The LEP ring showing proximity to Lake Geneva and electric rail lines. Also shown is ground current in the beam pipe. L3, Aleph, Opal and Delphi are at IPs 2, 4, 6 and 8. The circumference is 27 km.

Checking the electroweak radiative corrections was one of the central original motivations for the LEP program.

5.2. METHOD OF MEASUREMENT

Four detectors, Aleph, Delphi, L3, and Opal, use the LEP collider, shown in Fig. 11. The detectors need to identify the interactions with definable efficiencies, and tell the $\pm e^+$ direction. One concern is to measure the absolute luminosity; small high precision calorimeters are used to count small angle Bhabha (e^+e^- elastic) scattering. The experimental method has evolved sufficiently that the luminosity uncertainty is dominated by the QED calculation.[11]

A greater concern is the absolute beam energy calibration, which determines the precision of the Z mass measurement. Survey and field mapping, as for g-2, is not good enough by itself. The basic measurement uses res-

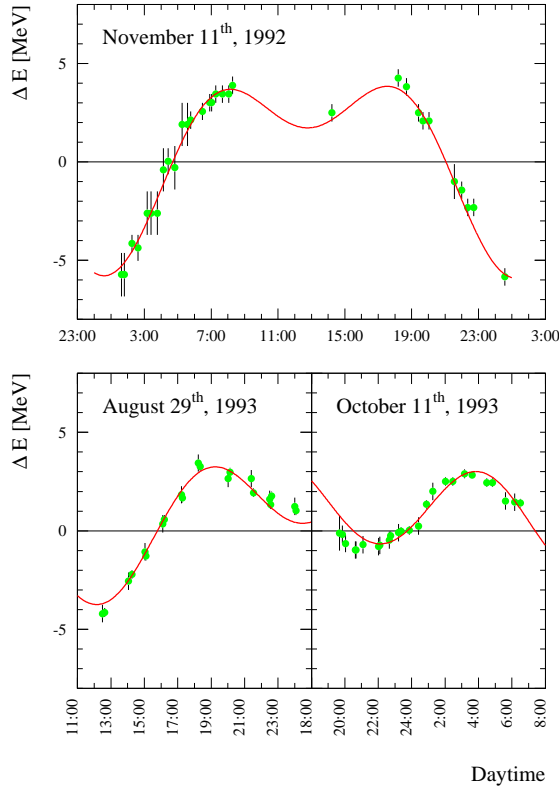


Figure 12. The LEP beam energy correlation to the moon, revealing the effect of tides.

onant depolarization.[12] With favorable accelerator parameters avoiding resonances, synchrotron radiation will tend to polarize the beams. Applying transverse RF, with precisely the correct frequency, causes the polarization to be lost. The intrinsic width for this procedure corresponds to 200 KeV. One corrects for RF energy gain and synchrotron radiation loss as appropriate from the measurement to each interaction point.

In practice, during energy scans, this measurement is made at the end of stores. The measurements show a 5 MeV spread in beam energy predicted from field and orbit measurements minus resonant depolarization values. If the depolarization measurement times are representative, one can combine them statistically to get absolute energy. But precision and confidence are improved if one can understand and model the time dependence which causes the spread.

The LEP program is clearly big science. The first correlation found was with the phase of the moon, shown in Fig. 12. The tidal expansion and contraction of the LEP ring is noticeable. Another influence on the

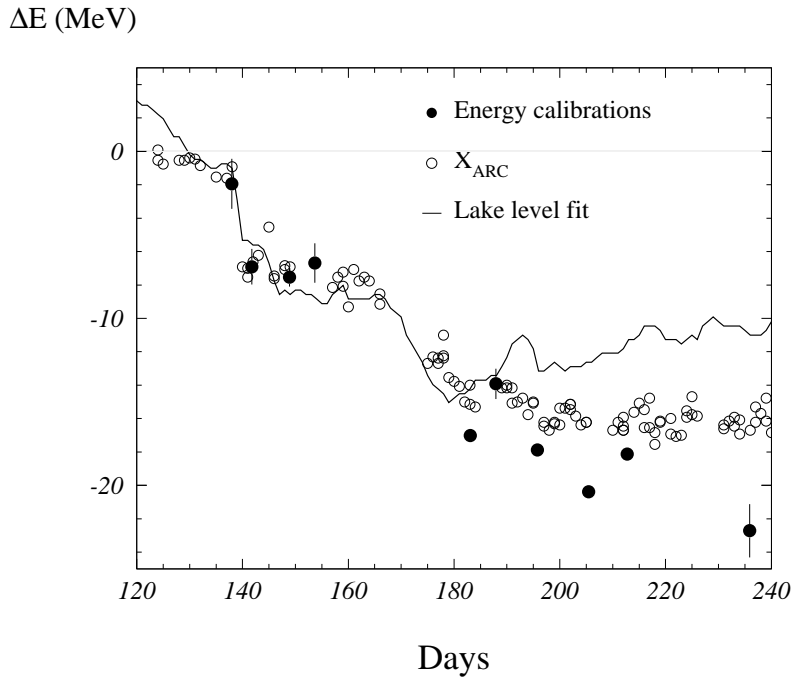


Figure 13. The LEP beam energy correlation to the water level of Lake Geneva.

size of the LEP ring is the amount of water in the ground; this is fairly well modelled by the water level of Lake Geneva, as see in Fig. 13. These correlations gave reasonable confidence in measurements through 1994.

A major energy scan was undertaken in 1995. During the run, unexpected time dependences were found in NMR readings. The patterns were found to be reasonably regular with daytime. Eventually these were found to be correlated with running of the TGV trains, as seen in Fig. 14. Apparently the TGV actually uses the ground to return current, and significant levels of current were found in the LEP beam pipe, shown in Fig. 11. A time dependent correction was determined, and a retroactive correction applied to previous data.

Charge asymmetries are straightforward to measure, although physics interpretation for hadrons can involve considerable sophistication in QCD and in relating jets to quarks and understanding charge correlations and efficiencies. The polarization of τ leptons is analyzed in the decay modes $\pi\nu$ and $\rho\nu$, as well as $a_1\nu$ and leptonic decays. The polarization angular

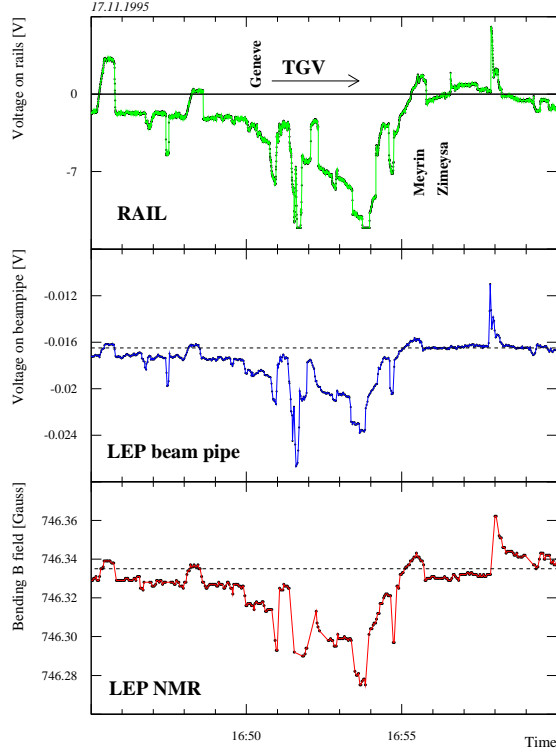


Figure 14. The LEP beam energy (NMR) correlation to current in the beampipe and power to the TGV.

distribution varies as

$$P_{\tau}(\cos\theta) = (A_{\tau}(1 + \cos^2\theta) + 2A_e\cos\theta)/(1 + \cos^2\theta + 2A_{\tau}A_e\cos\theta),$$

where $A_f \equiv 2g_V g_A / (g_V^2 + g_A^2)$ for Zf coupling.

5.3. RESULTS AND PROSPECTS

The L3 version of the Z scan is shown in Fig. 15. I will quote combined results from Vancouver 98.[13] The lineshape is well described by

$$m_Z = 91.1867(21) \text{ GeV}/c^2$$

$$\Gamma_Z = 2.4939(24) \text{ GeV}.$$

With efficiencies and luminosity normalization, one obtains a peak cross section of 41.491 (58) nb and an average leptonic decay width of 83.91 (10)

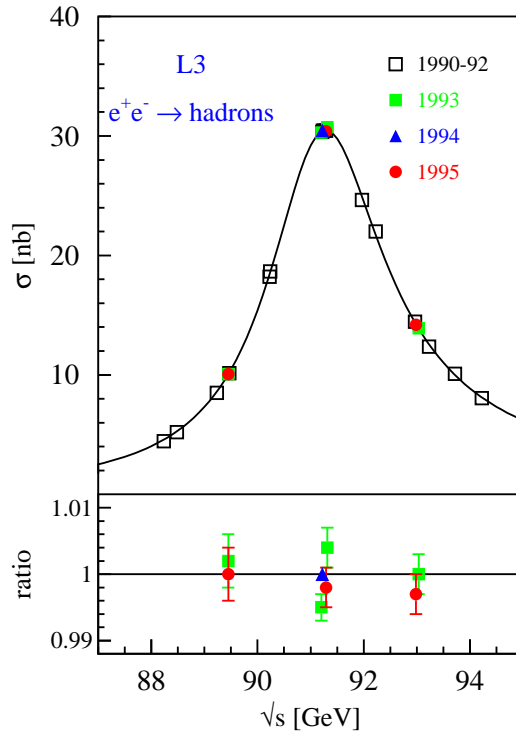


Figure 15. The LEP Z lineshape as seen by L3.

MeV. So there are three flavors of neutrinos, and no significant rate to any channel we don't know about.

The Z asymmetry measurements are summarized in Table 2. The leptonic measurements are a combination of $\mu^+\mu^-$ (most precise), with e^+e^- (diluted by t channel exchange), and $\tau^+\tau^-$ (lower efficiency). Of hadronic final states, the best measurement is for b quarks, as the tag tends to tell you where the quark really is. Identified charm and jet charge, which represents light quarks, have similar precision. Clearly, there are correlations among the hadronic measurements.

Gedanken Problem. Using several samples to make a given measurement, where there is cross talk between the samples, is a general problem. How do you deal with it?

The τ pair decay polarization angular distribution terms, which depend on electron and on tau coupling, are listed separately. All the asymme-

TABLE 2. LEP measurements of $\sin^2\Theta_{W_{eff}}$ from Z asymmetries.

Final state	Value	Error
Leptons	0.23117	0.00054
Jet charge	0.23210	0.00100
b jet	0.23223	0.00038
c jet	0.23200	0.00100
τ pol A_e	0.23141	0.00065
τ pol A_τ	0.23202	0.00057
Average	0.23187	0.00024

try measurements are reasonably consistent; split out as listed, the χ^2 per degree of freedom is 3.2/5.

The LEP1 data will not be significantly increased; the statistical impact of the occasional LEP2 Z calibration run is insignificant. Most analyses are reasonably mature. Some updates and refinements may be expected.

6. SLC Z Studies

6.1. GOALS OF THE MEASUREMENT

The goal of SLC is to use initial state electron polarization to give the most precise possible measurement of the Z asymmetry, and thus weak mixing. An overriding goal, not relevant here, is to demonstrate the feasibility of linear colliders.

6.2. METHOD OF MEASUREMENT

To measure the Z asymmetry A_{LR} , one simply measures the cross section difference for left- and right-handed electrons at the Z pole. All the detector needs to do is count events $(N_L - N_R)/(N_L + N_R)$, then divide out the beam polarization. The result depends on $\sin^2\Theta_{W_{eff}}$ as

$$A_{LR} = 2(1 - 4\sin^2\Theta_W)/(1 + (1 - 4\sin^2\Theta_W)^2).$$

The tricky part is obtaining and understanding the beam polarization.

SLC is shown in Fig. 16.[14] Positrons are made by accelerating electrons down most of the length of the linac, hitting a target from which positive charges are collected and returned to the start of the linac. After some acceleration, they are put into a damping ring.

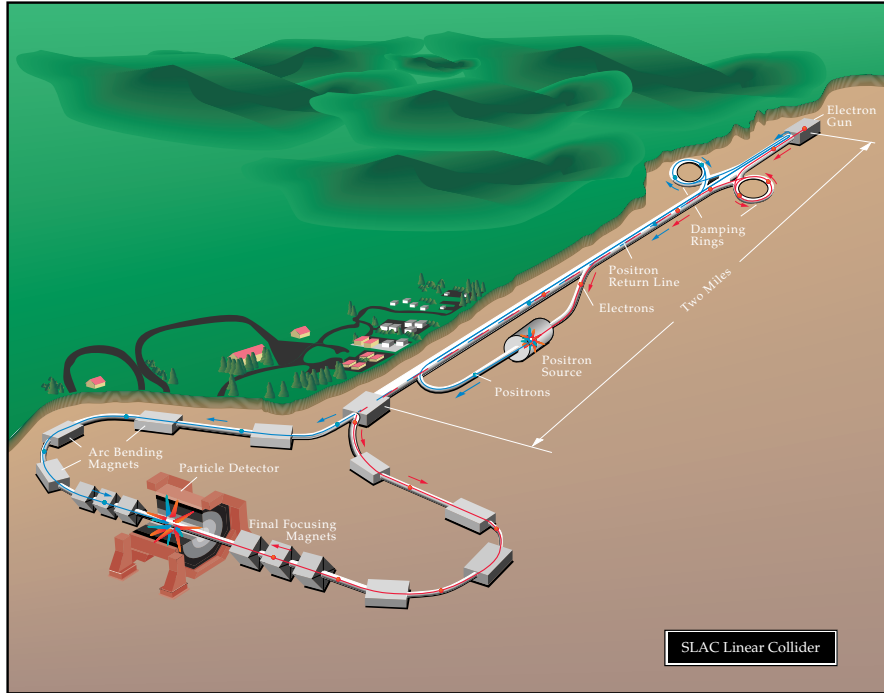


Figure 16. The linear collider at SLAC. The linac is 3.2 km long.

The polarized electron source was a great technical triumph. It produces right- or left-handed electrons based on a random number. These are accelerated a bit, then transferred, with spin rotated to vertical, to a damping ring. The damping rings are synchrotron radiation cooling rings, compressing the phase space of the electrons and positrons to allow a small beamspot and high luminosity.

For a pulse of the collider, the bunch of electrons, spin rotated back to longitudinal, are followed by the positron bunch, accelerated down the linac. At the end of the linac the electron polarization is rotated back to vertical for the arc, and checked with a Moller polarimeter. Preserving the polarization through the arc is also tricky, requiring delicate alignments. The polarization is rotated back to longitudinal going into the final focus and IP. The electron polarization is measured downstream of the IP with a Compton polarimeter, shown in Fig. 17; a Cerenkov detector array at several angles measures the asymmetry for recoil electrons which scatter off circularly polarized laser light.

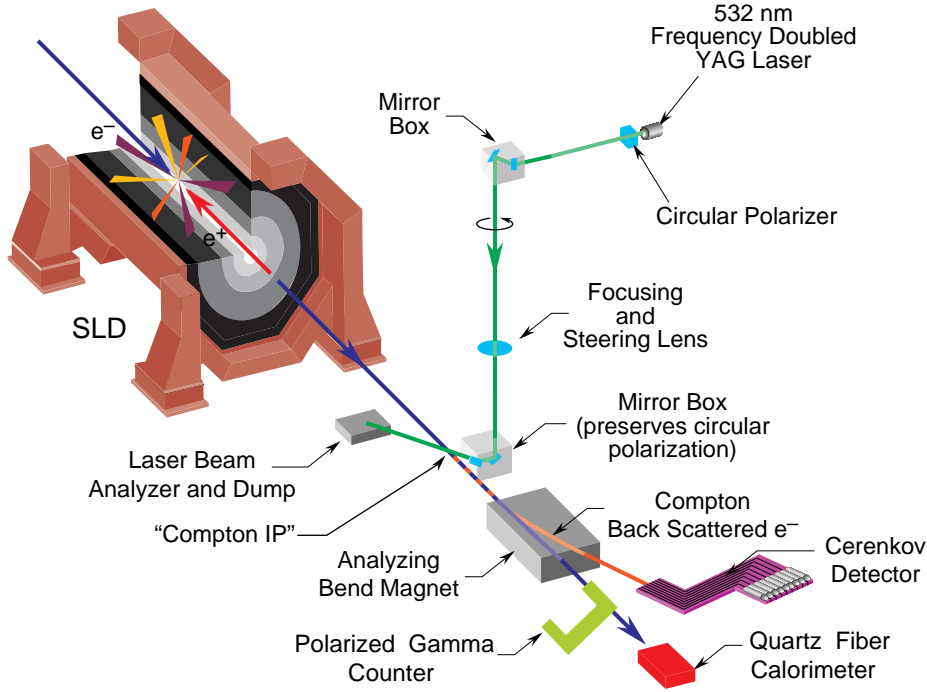


Figure 17. The Compton polarimeter.

A litany of systematic effects has been investigated, including laser polarization, noise, beam optics at the IP, bunch tails, and possible positron polarization. Everything seems to be under control. Average polarization is $77.25 \pm 0.52\%$.

6.3. RESULTS AND PROSPECTS

The result, as of Vancouver 1998,[15] is $A_{LR} = 0.1510 \pm 0.0025$; where the error includes $\sim \pm 0.0010$ systematics in quadrature. This gives $\sin^2\Theta_{W_{eff}} = 0.23101(31)$. This is indeed the most precise single measurement, and it continues the historic trend of being noticeably lower than other determinations. In combination with the LEP measurements one gets

$$\sin^2\Theta_{W_{eff}} = 0.23155(19).$$

With LEP itemized as listed in Table 2, this corresponds to χ^2 per degree of freedom of 8.1/6. So, in principle, a PDG S^* factor for combining measurements should be used to increase the combined error by $\sim \times 1.15$. In

previous years the consistency has been considerably worse, and in practice even the PDG struggles dealing with it.[16]

SLC/SLD has just completed running. They have some data not included above, and some systematic studies continue. A final update may come during 1999.

7. The Tevatron W Mass

7.1. GOALS OF THE MEASUREMENT

For a while, the only way to study W and Z bosons was at the $S\bar{p}pS$ collider at CERN. Parts of that program have continued at the Tevatron collider at Fermilab, remaining competitive in the LEP2 era. These include rare W decay searches, the W width, and of note here, the W mass. Each of the Tevatron collider experiments, CDF and DØ, would like to measure the W mass, with existing data, as well as any one LEP experiment will, $\sim \pm 100$ MeV/ c^2 . Eventually after running with the ongoing upgrades complete, each hopes to improve on the final LEP2 precision.

7.2. METHOD OF MEASUREMENT

When detecting e^+e^- collisions at the Z pole, if you see particles which vaguely correspond in energy to twice the beam energy, that is a Z . Vector bosons are readily produced in hadron collisions, but come in association with soft particles, which I will call “X” as in $\bar{p}p \rightarrow W + X$. Generally, Z and W bosons are observed at hadron colliders in leptonic decays.

X is made of low transverse momentum (few hundred MeV/ c^2) particles which evenly occupy longitudinal phase space, pseudorapidity $\eta = -\ln(\tan(\theta/2))$. For high luminosity, the inelastic cross section is large enough that extra “minimum bias” inelastic events overlap the events of interest. These events consist of soft particles distributed evenly in η . For the Tevatron running six bunches, 3.5 microseconds between bunches, an average of one overlap event corresponds to a luminosity of $\sim 6 \times 10^{30} \text{ cm}^{-2} \text{ sec}^{-1}$. The most recent Tevatron data had an average luminosity of almost twice that. As luminosity goes up, so does X. For the high luminosity upgrade, the luminosity will be spread out in more bunches, which will keep X down. At LHC, the bunches are 25 ns apart, but X gets rather large for luminosity anywhere near design.

W and Z production is described, as discussed by J. Stirling, by PDFs giving probabilities for finding partons in the proton and antiproton, and the Drell-Yan quark annihilation process.[17] QCD resummation[18] can be used to define parameters to describe $p_T(W)$ in the low $p_T(W)$ region relevant to measuring the W mass. These parameters are determined or

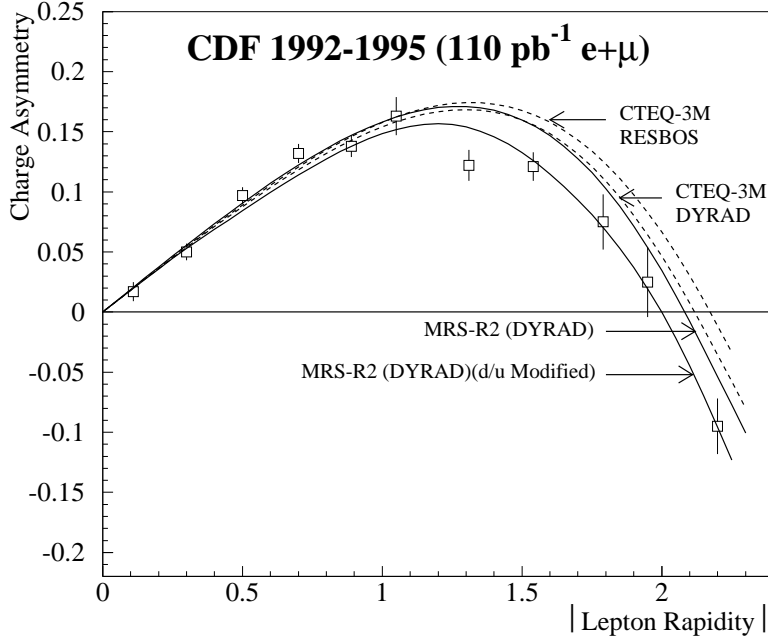


Figure 18. The CDF measurement of W lepton charge asymmetry. CTEQ and MRS are collaborations which do general fits for PDFs. DYRAD and RESBOS are NLO and resummed Monte Carlo generators respectively.

checked by measuring $p_T(Z)$. If $p_T(W)$ were perfectly predicted, then the p_T of the decay charged lepton would be used directly to estimate the W mass, minimizing the effect of X .

As pointed out in Stirling's discussion of PDFs, the momentum fraction distributions for u and d in the proton are different in shape. As W s are produced $u\bar{d} \rightarrow W^+$ and charge conjugate, there is a net W charge correlation, with W^+ tending to be produced with net longitudinal momentum along the proton direction. For central values of η , this charge correlation applies to the decay lepton, as seen in Fig. 18.[19] For higher absolute η , parity violation in the decay reverses the correlation seen in the decay leptons. Measuring this charge asymmetry gives a PDF constraint that is quite useful for measuring the W mass.

While the net longitudinal energy flow is essentially unmeasured, due to the finite longitudinal acceptance, the net transverse energy is reasonably well measured for modest X . The net calorimeter energy flow, other than the lepton, is the sum of response to the hadronic recoil against $p_T(W)$ and X . The neutrino is inferred from the net calorimeter imbalance. Typical W

event selection requires lepton and missing E_T above 20 GeV.

The optimal strategy for the W mass uses transverse mass,

$$m_T \equiv \sqrt{(E_T(\ell) + E_T(\nu))^2 - (\vec{p}_T(\ell) + \vec{p}_T(\nu))^2},$$

as the mass estimator; this minimizes the uncertainty resulting from variability of the $p_T(W)$ distribution.

Gedanken Problem. Under what circumstances is lepton transverse energy a better mass estimator than transverse mass?

In general, the Z sample can be used to calibrate all responses for measuring the W mass, but the cross section times leptonic branching ratio for Z s is an order of magnitude smaller than for W s.

The measurement depends crucially on calibrating the lepton energy scale. For the CDF magnetic detector this involves using $\psi \rightarrow \mu\mu$ to calibrate tracking, and understanding dE/dx and tracking systematics to extrapolate to the higher momenta of W and Z muon decays. The calibration is transferred to electron measurement by understanding the tracking material radiation length, and matching predicted E/p for W electrons. So far, for the most recent large data sample, CDF analysis is ongoing and only a preliminary muon result has been quoted.[20]

The DØ detector had no magnet for the data taken so far. They use the $Z \rightarrow ee$ mass with angular correlation, $\psi \rightarrow ee$, the π^0 mass, and the test beam measured linearity of their calorimeter to set the electron energy scale.[21] Taking $E(\text{measured}) = \alpha_{EM} \times E(\text{true}) + \delta_{EM}$, the constraints are shown in Fig. 19. For the final uncertainty, the deviation from linearity allowed by the test beam data is accounted, expanding the allowed region.

In reconstructing the recoil to $p_T(W)$, the DØ calorimeter reconstructs more than 80% of the net transverse energy. By contrast, CDF reconstructs slightly less than 60%. Most of the difference is due to the absence of a magnet in DØ; DØ has a statistical advantage due to the resulting better transverse mass resolution. The leptonic Z samples are used to calibrate this response.

Gedanken Problem. Do you know of any instance when making a compensating calorimeter (DØ as opposed to CDF, ZEUS as opposed to H1), as discussed by J. Virdee, created an actual physics measurement advantage?

There is no analytic form to describe the transverse mass distribution, shown for the DØ 94-95 data in Fig. 20. A fast Monte Carlo generator including all that is known about W production and detector response is used to make transverse mass templates as a function of assumed W mass.

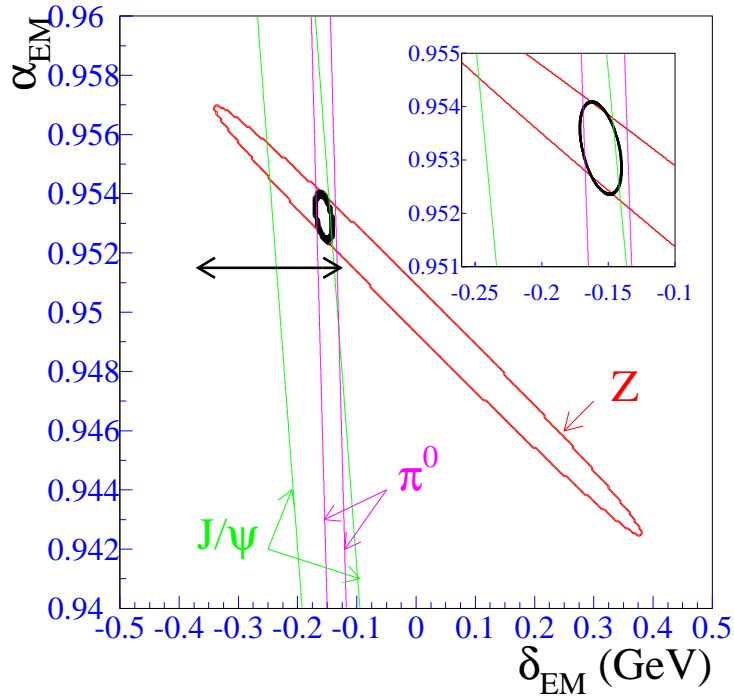


Figure 19. The D0 electron energy scale determination. α is the scale and δ is the effective pedestal offset.

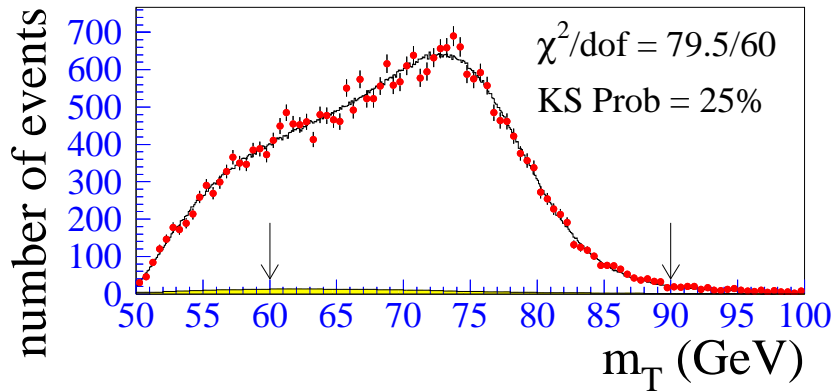


Figure 20. The D0 electron W transverse mass distribution. The fitting region is marked, as is the small background contribution.

The templates are then used in a likelihood fit. We will see this procedure of fitting data to Monte Carlo templates several times.

7.3. RESULTS AND PROSPECTS

TABLE 3. Measurement errors in MeV/c^2 for the 94-95 DØ W mass determination.

Statistics	95
Lepton systematics	35
Recoil measurement	40
QCD model (PDF, resum)	25
QED radiative cor.	15
Background	10
Other	15
ALL systematics	70
ALL	120

DØ has completed and published their analysis.[21] The errors are listed in Table 3. Note that the 95 MeV statistical error includes, in quadrature, 65 MeV for Z statistics in setting the electron energy scale. The overall modelling (theory) error is at the level of $\sim \pm 30$ MeV which bodes well for the future.

They measure $m(W) = 80.44 (12) \text{ GeV}/c^2$ for 94-95 data, and $80.43 (11)$ when combined with their earlier data. The preliminary 94-95 CDF muon measurement gives $80.43 (16)$, and combined with previous measurements gives $80.38 (12)$. Combining DØ, CDF, and UA2, and accounting common uncertainties, gives $m(W) = 80.41 \pm 0.09 \text{ GeV}/c^2$.

DØ has reached its goal, while CDF is still working on theirs. Both detectors are undergoing major upgrades; “run 2” data taking should begin in 2000. A solenoid and magnetic tracking is part of the DØ upgrade. The accelerator upgrade includes the Main Injector and much improved antiproton collection. More bunches will be used to spread out the increased luminosity, the six bunches for existing data (“run 1”) will increase to 36 and eventually to ~ 100 bunches.

The run 1 existing datasets correspond to $\sim 110 \text{ pb}^{-1}$. By 2003 each experiment hopes to collect $2\text{-}4 \text{ fb}^{-1}$. Further improvements could produce samples of perhaps 20 fb^{-1} by the end of 2005. Such samples should allow the final LEP2 W mass precision of $35\text{-}40 \text{ MeV}/c^2$ to be seriously challenged.

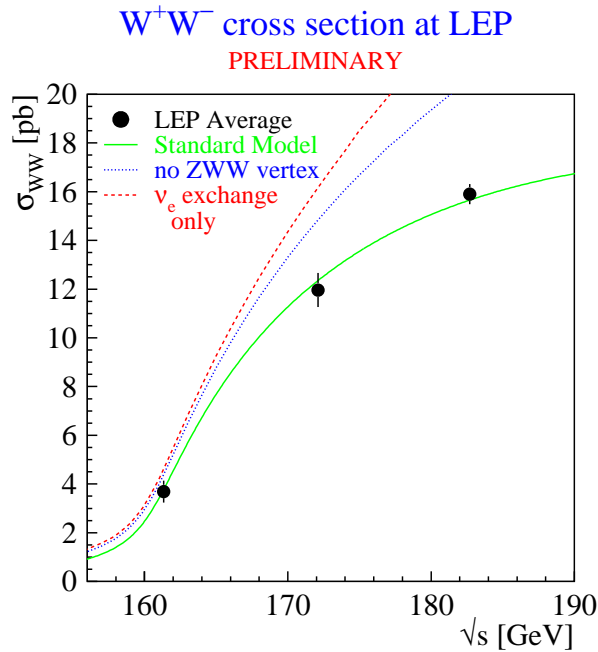


Figure 21. The W pair cross section at LEP.

8. The LEP2 W Mass

8.1. GOALS OF THE MEASUREMENT

The twin goals of the LEP2 program are the study of W bosons and searches. Part of the former is a goal for an eventual combined W mass determination to $40 \text{ MeV}/c^2$ or better. My discussion of progress toward this goal will follow the recent review by Glenzinski.[22]

8.2. METHOD OF MEASUREMENT

With increased RF available, the energy of the LEP ring has risen sufficiently to allow $e^+e^- \rightarrow W^+W^-$. The initial W mass measurement came from running just over threshold and measuring the cross section, just as the τ mass was precisely measured at BES.[23] The left-most point in Fig. 21 best determines how much the solid curve can slide horizontally. This threshold analysis is statistically limited, but the drive to search for new things raised the energy and changed the strategy to direct reconstruction.

The most important channels for direct reconstruction are both W s decaying hadronically, “ $qqqq$,” or else one decaying hadronically and the

other producing an electron or muon, “ $\ell\nu qq$.” Some collaborations include $\tau\nu qq$, but I will ignore that complication. Lepton measurements and net energy flow have been discussed previously. The identification of jets of energy flow with final state partons was discussed by Stirling. The LEP collaborations typically use the JADE[24] and DURHAM[25] algorithms for this analysis.

The analyses use kinematic constrained fits. These apply energy and momentum conservation to a set of measurements that can be pulled within their measurement errors, defining a χ^2 . For the $qqqq$ case, energy conservation means the energy of each W is given by the beam energy, neglecting initial state radiation (ISR). The electron or positron is likely to radiate a photon down the beampipe before interacting, calculable in QED. Each component of momentum should sum to zero; in the z or beam direction this again implies neglecting ISR. So one assigns the energy flow to four jets, hypothesizes two pairs as making up each of the 2 W s (there are three choices), and calculates a χ^2 for the hypothesis.

In addition to the four constraints (4C) above, one may constrain the two separate W masses to be the same within an error which includes the effect of $\Gamma(W)$, 5C. When good enough solutions are found, either the lowest χ^2 solution, or a weighted average of acceptable solutions, is used to give the mass measurement for that event. The distribution of measurements is fit to Monte Carlo templates varying the assumed W mass; the Monte Carlo includes the ISR neglected in fitting. Four jet W pair candidates are typically selected with an efficiency of $\sim 85\%$ and a purity of $\sim 80\%$. This is illustrated by the ALEPH $qqqq$ data at 183 GeV shown in Fig. 22.[26]

The event selection for $\ell\nu qq$ is typically $\sim 87\%$ efficient and 95% pure. Since net momentum measurement must be used for the neutrino, we are left with one constraint, or two for equal W masses. This channel is illustrated for ALEPH $e\nu qq$ data at 183 GeV in Fig. 23.[26] Note that in both cases, the use of the beam energy makes the result less sensitive to absolute jet energy measurement systematics.

Gedanken Problem. Why is there a tail on the high side in Fig. 23? Does raising the LEP energy help the W mass measurement by direct reconstruction?

The DELPHI collaboration uses a somewhat different approach, as discussed in the talk by Martijn Mulders. They attempt to measure ISR event by event, and fit reconstructed mass to an analytic form.[27]

LEP runs at the Z from time to time to help monitor detector responses.

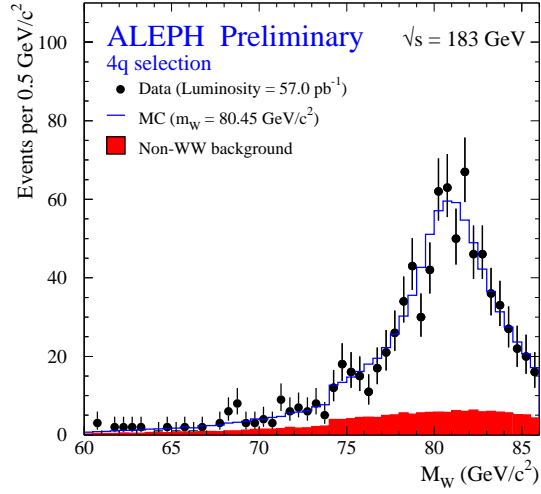


Figure 22. The ALEPH W mass reconstruction at 183 GeV in $qqqq$.

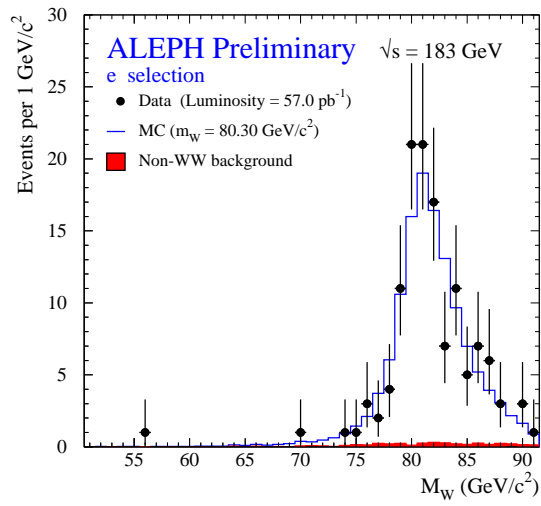


Figure 23. The ALEPH W mass reconstruction at 183 GeV in $e\nu qq$.

TABLE 4. ALEPH 183 GeV W mass systematics in MeV/c^2 . Those marked * are correlated in all experiments.

SOURCE	$\ell\nu qq$	$qqqq$
ISR*	5	10
Hadronize*	25	35
Detector	22	24
Fit	15	14
Beam energy*	22	22
CR/BE*	-	56

8.3. RESULTS AND PROSPECTS

ALEPH preliminary systematic errors for 183 GeV measurements are given in Table 4.[26] “Hadronize” refers to the systematics of associating measured energy with final state partons, including soft gluons. Detector effects include boundaries and linearity. The fit error includes selection biases, background uncertainties, and Monte Carlo statistics. “CR/BE” refers to QCD final state correlations: color reconnection, as the W s decay so quickly that decay parton color fields from both W s overlap, and Bose-Einstein correlations for final state pions from both W s. Such final state correlations are being looked for, and can be measured or limited.

The 183 GeV measurements, quoted at Vancouver for the combined LEP experiments[13] are $m(W) = 80.28$ (12) for $\ell\nu qq$ and 80.34 (14) for $qqqq$. The overall direct reconstruction result is 80.36 (9). Combining that with the threshold measurement of 80.40 (20) gives $m(W) = 80.37(9)$ for the overall LEP2 direct measurement. Combining this with hadron collider measurements one obtains

$$m(W) = 80.39 \pm 0.06 \text{ GeV}/c^2$$

as the overall direct measurement, with if anything, a shortage of χ^2 in combining results.

The LEP2 run is just getting started. Progress is being made on systematics so that by the end of the run in 2000, the desired precision looks possible.

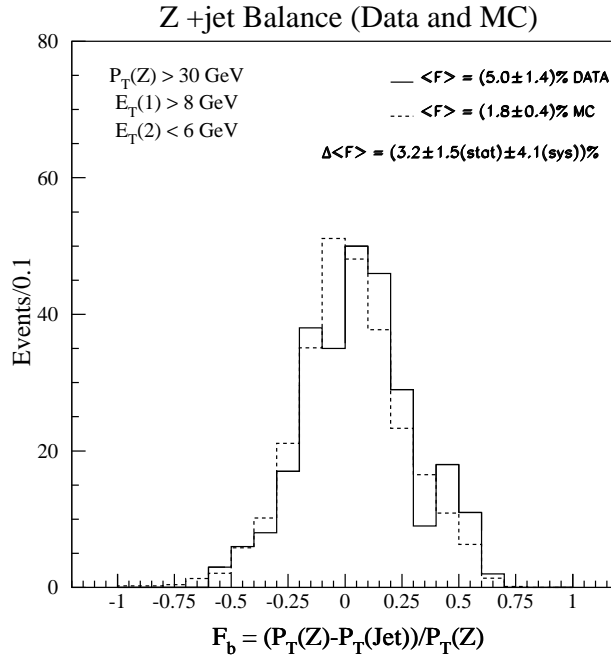


Figure 24. The Z jet balance: lepton p_T minus jet p_T over lepton p_T for CDF $Z + jet$ events, data and Monte Carlo.

9. The Tevatron Top Mass

9.1. GOALS OF THE MEASUREMENT

Having established the presence of the top pair signal, the goals are to confirm the characteristics of that signal in all possible ways and relevant here, to measure the top mass as accurately as possible.

9.2. METHOD OF MEASUREMENT

At the Tevatron, top is predominantly pair produced in the subreaction $\bar{q}q \rightarrow g \rightarrow t\bar{t}$. Top decays are essentially 100% to Wb , so the final state for top pairs contains two W s like LEP2, a b and \bar{b} , and of course, X . Like LEP2, the channels are characterized by the W decays, again taking leptons as e or μ , all hadronic “ $qqqbb$,” lepton plus jets “ $lvqqbb$,” and dilepton “ $lvlvbb$.” The all hadronic channel has relatively poor signal-to-noise. The dilepton channel has poor statistics, and is underconstrained due to the two neutrinos, and thus is tricky. I will discuss the lepton plus jets channel, which gives most of the precision.

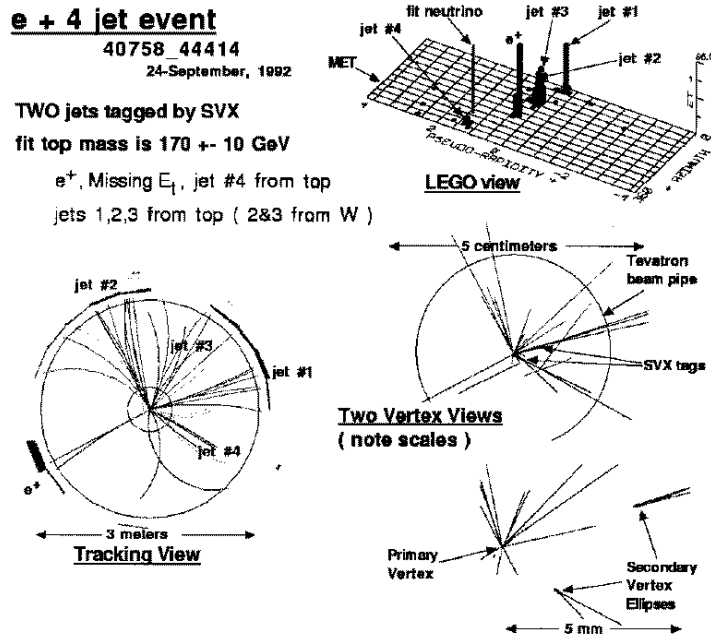


Figure 25. A reasonably convincing CDF electron plus four jet top candidate. The LEGO view shows calorimeter energy in $\eta \times \phi$; the other views are in ϕ .

This measurement is based on jet energies, without the beam energy calibration possible at LEP. Jets are defined as calorimeter clusters of energy in a circle (“cone”) in $\eta \times \phi$ space of radius typically ~ 0.4 . We have seen, in the W mass discussion, the EM calorimeter calibration. For CDF, the hadronic calibration starts from the test beam, then uses jet fragmentation, with the nonlinearity of calorimeter response measured from test beam and *in situ* isolated particle measurements. There are corrections for final state hadrons coming from the relevant parton falling outside the cone, and for X getting into the cone. As luminosity varies, X varies, which can be corrected on average for a given sample; there is also a jet threshold bias. These effects are studied by combining top events, real and Monte Carlo, with one or more minimum bias events.

The detailed jet response study is done with the help of tracking, that is for calorimeters covering central rapidity. The scale is transferred to the rest of the calorimeters using dijet balance. The process can be checked

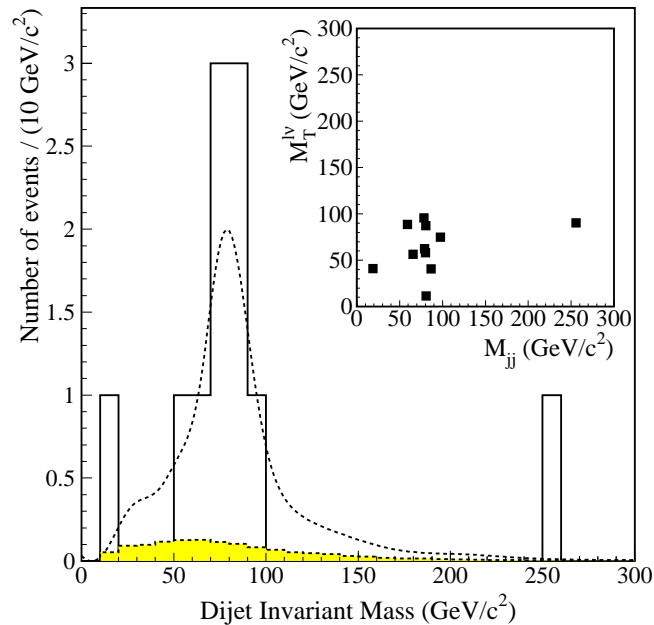


Figure 26. The untagged two jet mass for CDF lepton plus 4 jet events where two jets have loose SVX tags, and the correlation of that with the transverse mass reconstructing the leptonic W . The curve is Monte Carlo prediction with the shaded area background.

using photon/jet event balance, but one needs to worry that selecting or triggering on a photon puts an initial state intrinsic transverse momentum “ k_T ” bias. The initial partons tend to be moving in the photon direction. Top specific jet corrections account mostly for muons in b decays. The final check that this all makes sense is to look at the transverse energy balance in $Zjet$ events. This is shown in Fig. 24 for CDF Z events, where the lepton pair p_T is above 30 GeV/c. This is balanced essentially by one jet, with no other jet above 6 GeV E_T . The agreement is well within the expected systematic error.

$D\bar{O}$ employs an equivalent procedure, starting from the electromagnetic scale and studying photon jet balance etc. Although with no magnet, they have fewer handles but their corrections are smaller.

For obtaining a mass estimate, kinematic fitting is again used. One starts with a sample of events with a lepton plus four jets and missing E_T . Only overall transverse momentum balance is available, and that is used to define the neutrino p_T . The longitudinal momentum of the neutrino is unmeasured. There are two W mass constraints, one on a jet pair and

the other on the lepton and the inferred neutrino. There are usually two viable constraint solutions for the neutrino longitudinal momentum (“ambiguity”). A further constraint comes from demanding that the two top masses be consistent. The net constraint is $2C$.

The fit is well illustrated by considering an event, shown in Fig. 25, where two jets are identified as bs by silicon vertex tags (“SVX”). Jets 2 and 3 seem together in the calorimeter display, but are clearly separated in the tracking view. The secondary vertices at a few mm identify jets 1 and 4 as bs . Thus jets 2 and 3 should be a W ; the invariant mass of the pair, not fit, is $79 \text{ GeV}/c^2$. The only ambiguities are: which b goes with which W , and which neutrino solution to use. The best χ^2 assigns jet 4 to the leptonic W , and gives an event top mass of $170 \pm 10 \text{ GeV}/c^2$. The W s observed for all candidates events, when there are two loose SVX tags, are shown in Fig. 26. With enough statistics the W peak may become a calibration.

If you don’t have the b tag information, you simply try all the possibilities. Sometimes the best χ^2 is the wrong combination; the top mass resolution degrades as the number of possible combinations grows. Both CDF and $D\bar{O}$ tag b jets using associated e or μ from heavy quark decay, called soft lepton tag, SLT. The statistics, signal and background levels, and resolution are illustrated for CDF in Fig. 27. In defense of the SLT sample, it should be noted that SLT tagged events that are also SVX tags are removed from the SLT sample and kept as SVX, just as all tagged events have been removed from the no tag sample.[28]

$D\bar{O}$ defines four variables, with minimal mass bias, that discriminate the top from the background. The background is predominantly $W + jets$ with some fake leptons. The variables are missing E_T , acoplanarity, the centrality of the non-leading jets, and a measure of the smallest 2 jet separation. They do a joint fit to a discriminant or a neural net (NN) output constructed from the four variables, and top mass, as illustrated in Fig. 28. The discriminant and neural net analyses are combined, accounting correlations, to give their result.[29] The combination uses the technique of pseudoexperiments, analyzing many Monte Carlo samples of the same size as the data to understand measurements and correlations. Such exercises allow you to understand whether a given fit result makes sense.

9.3. RESULTS AND PROSPECTS

The several top mass determinations are listed in Table 5. The predominant systematic error comes from the jet energy scale. This is $\sim \pm 5 \text{ GeV}/c^2$ in lepton plus jets. It includes jet systematics, as discussed, as well as variation with different assumptions about how much gluon radiation goes where. With enough data, even the gluon variation can be constrained. The

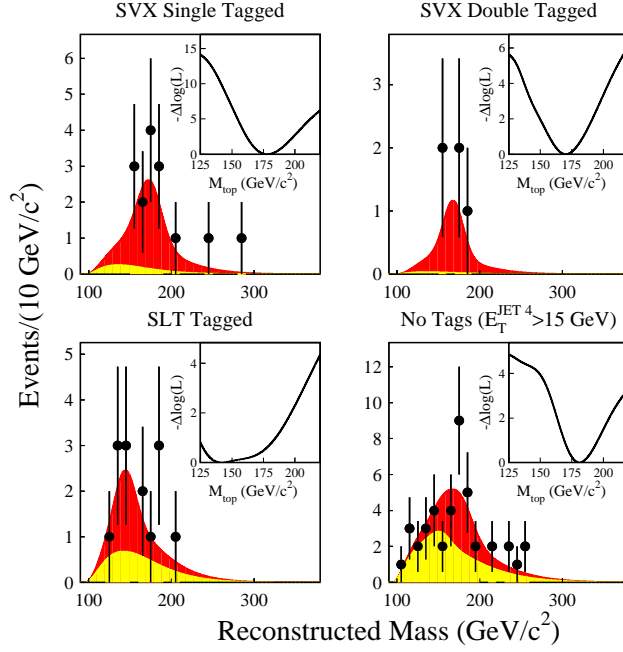


Figure 27. CDF top mass distributions and fits for the SVX 1 tag, SVX 2 tag, SLT tag and no tag samples. The insets are likelihood results. The shaded areas are the fit results with dark signal and light background.

TABLE 5. Top mass measurements, in GeV/c^2 .

Channel	Experiment	Value
$lvqqbb$	CDF	175.9 ± 6.9
$lvqqbb$	DØ	173.3 ± 8.4
$lvlvbb$	DØ	168.4 ± 12.8
$lvlvbb$	CDF	167.4 ± 11.4
$qqqqbb$	CDF	186 ± 13

several results have been combined,[30] accounting correlations, to give

$$m(\text{top}) = 173.8 \pm 5.0 \text{ GeV}/c^2$$

Only minor refinements to the analysis of existing data may be expected.

It is difficult to predict how much improvement can be achieved with the Tevatron upgrades, given the jet energy scale systematic level. But our

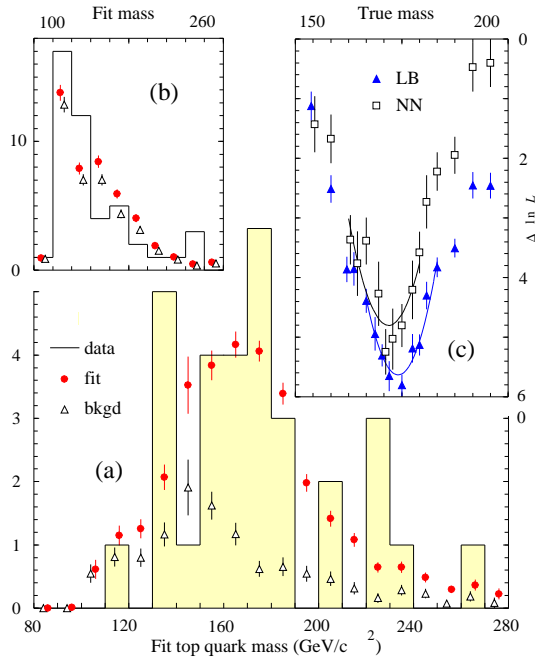


Figure 28. $D\bar{0}$ top mass distribution and fit for (a) predominantly signal events and (b) predominantly background events. The likelihoods for the two discriminants are shown in (c).

measurements with $\sim 110 \text{ pb}^{-1}$ are almost as precise as we predicted a few years ago for the upgrade 2 fb^{-1} samples.[31] A factor of two improvement seems reasonably safe, for twenty times the data with improved detectors.

10. The LEP2 Higgs Search

10.1. GOALS OF THE MEASUREMENT

One of the accomplishments of the LEP program has been to search for the Standard Model Higgs over the complete kinematically allowed range of the Higgs mass. So far nothing has been found. In the LEP2 era, as the energy rises the search is extended, typically to twice the beam energy minus the Z mass. As an illustration, I will describe the L3 analysis of the 183 GeV data.[32]

10.2. METHOD OF MEASUREMENT

For incrementally adding at the high end of the Higgs search, the relevant process is $e^+e^- \rightarrow Z^* \rightarrow HZ$, where $H \rightarrow \bar{b}b$ since bs are the heaviest available decay mode. The final states looked at, listed as HZ , are $bbqq$, $bb\nu\nu$, $bb\ell\ell$, $\tau\tau qq$ and $bb\tau\tau$. Given the four competing experiments, the analysis is fairly sophisticated. A sample is selected with cuts, a neural net (NN) discriminant is used to characterize Higgs signal versus background, as in the D0 top mass analysis, independent of mass. A candidate sample is checked as a function of mass and the mass information is used in defining a purity used to set a limit. The various channels are combined for a final result.

Gedanken Problem. What are the good and bad points of having several competing experiments? How many are appropriate?

For the $bbqq$ mode, the initial sample is JADE algorithm[24] 4 jet events. Further selection is based on tracks, calorimeter clusters, visible energy, small net energy flow, and no lepton or photon candidates. Energy is apportioned to the jets with the DURHAM algorithm[25] and a 4C fit defines a kinematic χ_{fit}^2 . How well an appropriate jet pair gives a Z mass determines the selection on a χ_{mass}^2 . The 321 events selected compare to 315 predicted for background, mainly W pairs and $qq\gamma$. For the NN, tracks, clusters, event shape, b tag and χ_{fit}^2 are used. The results are shown in Fig. 29. Twenty events have $NN > 0.5$, but there is no sign of any signal.

For the $bb\nu\nu$ mode, events are selected on tracks and clusters. Two jet events (DURHAM) with a recoil mass between 40 and 115 are consistent with $Z \rightarrow \nu\nu$. Net energy flow and b tag probability are required. The 56 events found compare to 50 predicted as background. The NN uses b tag, angles, recoil mass, jet masses, net E_T and χ_{fit}^2 . The results are shown in Fig. 30. Again there is no sign of a signal.

For the $bb\ell\ell$ mode, where ℓ as usual is e or μ , the Z is observed as the lepton pair; 6 ee candidates and 2 $\mu\mu$ candidates are found, again consistent with background. The NN uses b tag, angles, $m(Z)$, jet masses, and χ_{fit}^2 . Only one event has $NN > 0.1$; it gives a mass less than 70.

For the two $\tau\tau$ modes, τ s are selected as two isolated 1/3 prongs of opposite charge. A cut discriminant uses jets, angles, masses, b tag and χ_{fit}^2 . One event is selected with a predicted background of 2.4.

There is no sign of a signal and systematics are included in a pseudoexperiment exercise for combining channels. Systematics include luminosity (0.3%), detector efficiency (4%) and background uncertainty, taken as correlated between channels (10%).

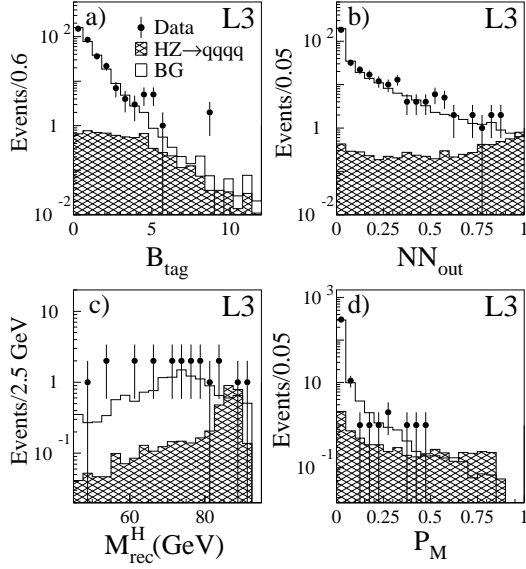


Figure 29. For $bbqq$; the b tag discriminant (a), NN output (b), H mass for the events with $NN > 0.5$ (c) and purity (d). The open histogram is background, and the shaded one is a nominal 87 GeV Higgs signal.

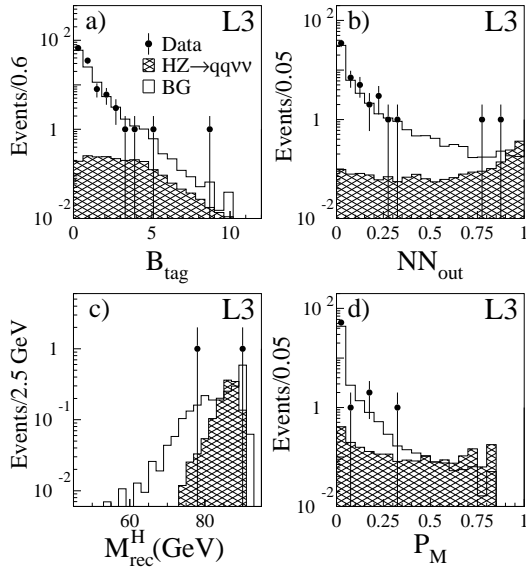


Figure 30. For $bb\nu\nu$; the b tag discriminant (a), NN output (b), H mass for the two events with $NN > 0.5$ (c) and purity (d). The open histogram is background, and the shaded one is a nominal 87 GeV Higgs signal.

10.3. RESULTS AND PROSPECTS

The L3 analysis sets a limit $m(H) > 87.6 \text{ GeV}/c^2$ at 95% CL. The pseudo-experiment study gives a probability for obtaining a higher limit given the data sample of 35%, so they did not get too lucky. The overall LEP2 limit is[33]

$$m(H) > 89.8 \text{ GeV}/c^2 \text{ 95\% CL.}$$

Considerably more luminosity is expected for LEP2, but more important for this search, the energy should get up to 200 GeV. Thus, the limit could get up to 109, or else a signal could be well established up to $99 \text{ GeV}/c^2$.

A further window for the Higgs search to about $120 \text{ GeV}/c^2$, will be available at the upgraded Tevatron if that collider produces data samples of $\sim 20 \text{ fb}^{-1}$. There, one hopes to see $\bar{q}q \rightarrow W^* \rightarrow HW \rightarrow bbl\nu$. It would be interesting to observe HW if HZ is found at LEP, a possibility which should be kept in mind. Beyond that, the possibilities are rather thoroughly covered by LHC, as discussed by F. Pauss.

11. Conclusions

The program of precision electroweak measurements is a great success since all the measurements are consistent. The simple-minded minimal Higgs scenario is still allowed. If the motivation was to get beyond the limitations of the Standard Model by detecting a contradiction, then we must report failure.

11.1. DIGRESSION ON TOPICS NOT COVERED

Before we get into global fits, a few measurements need to be mentioned. The decay fraction of Z to $\bar{b}b$, R_b , has an interesting history; the formerly exciting discrepancy is now merely a slight pull toward lower top mass. While Z asymmetry measurements dominate the overall Higgs mass constraint, with W mass in a distant second place, the Z width and leptonic branching fractions also have some influence.

One can search for new physics in the trilinear couplings, *eg.* ZWW . While the destructive interference in W pair production was demonstrated at the Tevatron,[34] the Tevatron constraints[35] are being overtaken by the LEP2 studies.[13]

The W branching ratios are now being directly measured at LEP2. The leptonic fractions will soon be more precise than the Tevatron constraints from the leptonic Z/W cross section ratio. The Tevatron still has much larger samples, given a trigger signature, and continues to have the more accurate direct W width measurement, and better reach for rare W decays.

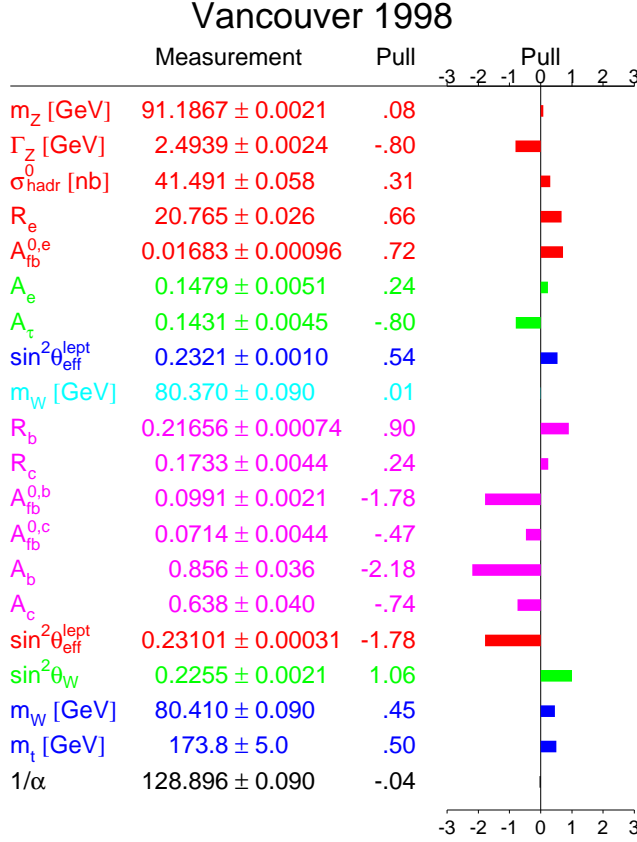


Figure 31. The summer 1998 LEPWWG global fit pull distribution. The top 15 measurements are combined LEP results, then SLD, NuTeV, two from the Tevatron Collider, and calculated α . The fit also gives an α_S in agreement with other measurements.

I also note that in many cases flavor universality is tested as well as assumed. Axial and vector couplings can be measured separately, and many assumptions can be relaxed and checked.

11.2. GLOBAL FITS

Although the $g-2$ experiment may not soon provide input to the global electroweak fits, all the other measurements discussed do. I will use the LEP-EWWG version as quoted at Vancouver; [13] PDG gets similar results. [16] That it all hangs together is shown in the pulls plot, that is how much each measurement deviates from the fit value, Fig. 31. The usual suspects are off a bit, but none have either the statistical significance or the connection

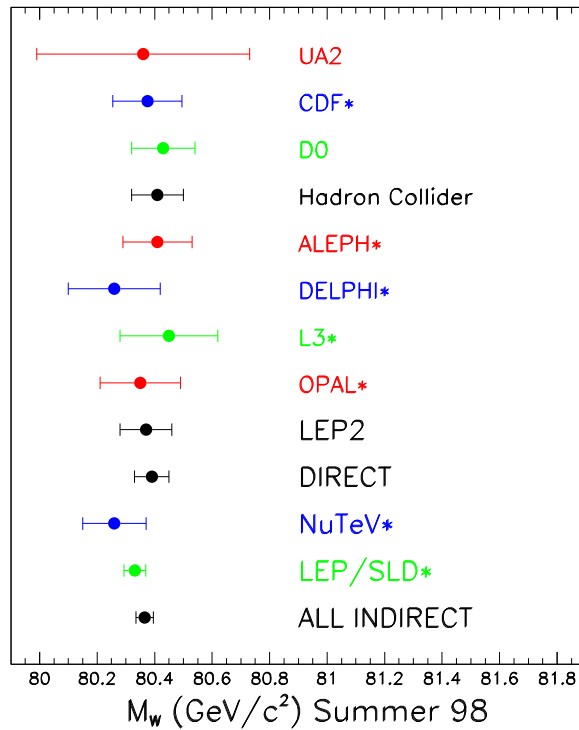


Figure 32. The summer 1998 W mass determinations, direct and indirect. Measurements marked * include preliminary results.

to a popular SUSY scenario to make them noteworthy.

Let us check if the W mass, calculated indirectly through radiative corrections, agrees with the direct measurements. This is shown in Fig. 32. The direct measurements agree among themselves, perhaps too well. The NuTeV analysis inputs the measured top mass, while LEP/SLC does not; they also indirectly infer a top mass. For the global indirect W mass, the direct top mass measurement is included, moving the result up.

If utility is defined as providing the greatest constraint on the Standard Model Higgs mass, then given the incredibly precise measurements of α , G_F and $m(Z)$, the Z asymmetries are most useful. This constraint is illustrated in Fig. 33. While a couple of individual measurements would prefer the Higgs to have been found some time ago, the general trend can accommodate a Higgs mass such that there is no need for new physics to the Planck scale.

The correlation of the W mass and the top mass is shown, in the NuTeV world view, in Fig. 34. The Z asymmetry dominates the width of the region

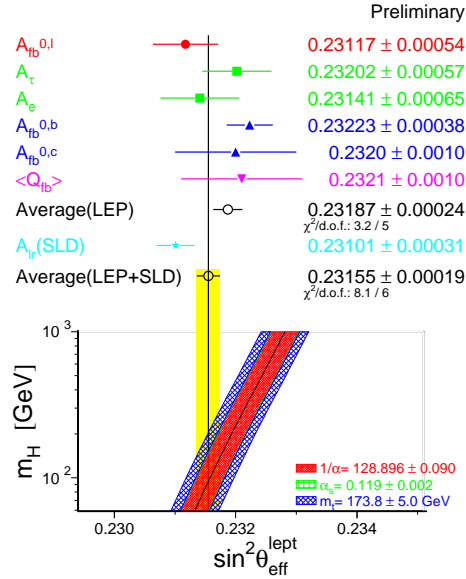


Figure 33. The summer 1998 LEP/SLD Z asymmetry measurements.

allowed by LEP/SLC indirect measurements as $m(H)$ changes. A factor of two improvement on both direct measurements will help a lot.

The overall Higgs constraint is shown in Fig. 35. This is quoted as giving a one-sided 95% CL upper limit on the Higgs mass, increased since Moriond 1998, of $280 \text{ GeV}/c^2$. [36] But one should not really ignore the fact that the left side of the plot has been ruled out. Even in the most unfavorable MSSM scenario, SUSY Higgs below $70 \text{ GeV}/c^2$ are ruled out. [37] It may be more appropriate to call the limit $\sim 90\%$ CL; 5% of what is left on the right side of the plot corresponds to a rather higher mass limit. No allowance has been made for measurement discrepancies; the limit depends strongly on the SLD A_{LR} result. So the SUSY establishment, hoping that the presence of a low mass Higgs will be established, needs to remain patient.

The simplest Standard Model Higgs scenario remains viable. Except for those SUSY scenarios which imitate the Standard Model, more complicated Higgs scenarios generally imply that there is no constraint.

Gedanken Problem. Using all the information about Fig. 35, and avoiding religious prejudice, what would you quote for a Higgs mass upper limit?

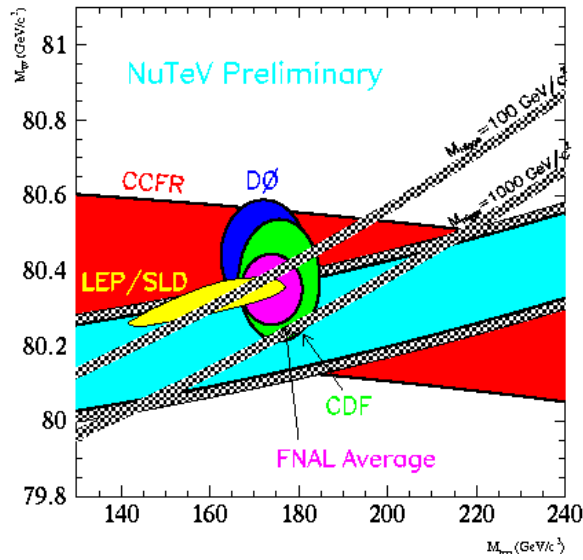


Figure 34. The parameter space of W mass and top mass, with bands shown for Higgs mass values and contours showing measurement constraints.

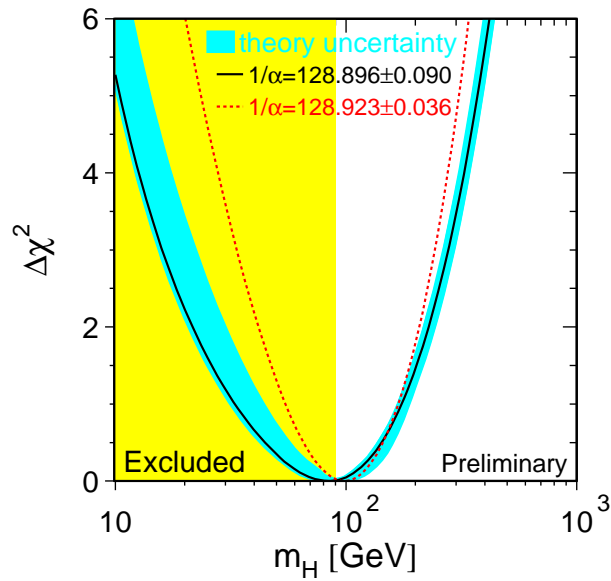


Figure 35. The global electroweak fit χ^2 versus Standard Model Higgs mass value.

11.3. PROSPECTS

The BNL g-2 experiment is just getting started. LEP1 and SLC have finished running, with some analysis updates pending. LEP2 is just getting going and one can anticipate W mass precision improvements, as well as an extension of the Higgs search in what seems to be a promising region.

The Tevatron is on hiatus, upgrading. Some updates, particularly on the W mass, are pending. Once Tevatron running resumes, substantial improvements may be expected in top mass and W mass precision, giving these measurements comparable electroweak precision to the Z asymmetries. There is even some window of opportunity to search for $H \rightarrow \bar{b}b$, slightly extending the LEP2 range.

If we are persistent and patient, LHC results must eventually clarify the picture. I certainly hope that we learn something more than a value for the Standard Model Higgs mass.

12. Acknowledgements

I thank Tom Ferbel for being our perfect host. I am grateful to the students, and to my fellow lecturers for keeping things so interesting. I would like to thank Cosmas Zachos, Lee Roberts, Doug Glenzinski, Jae Yu, Randy Keup, Darien Wood, Alain Blondel and Ruth Hill for their help. This work was supported in part by the U. S. Department of Energy, contract W-31-109-ENG-38.

References

1. S. Weinberg, Phys. Rev. Lett. **19**, 1264 (1967); A. Salam in *Elementary Particle Theory*, ed. N. Svartholm (Almquist and Wiksells, Stockholm 1969) p. 367.
2. J. Bailey *et al.*, Nucl. Phys. **B150**, 1 (1979).
3. L. Roberts, Proc. ICHEP96 (Warsaw), ed. Z. Ajduk and A. K. Wroblewski (World Sci., 1997) pp 1035-1039.
4. A. Czarnecki, B. Krause and W. Marciano, Phys. Rev. Lett. **76** 3267 (1996).
5. A. Czarnecki, B. Krause and W. J. Marciano, Phys. Rev. **D52**, R2619 (1995).
6. R. Alemany, M. Davier and A. Höcker, Eur. Phys. Jour. **C2**, 123 (1998), M. Davier and A. Höcker, Phys. Lett **B419**, 419 (1998).
7. M. Hayakawa and T. Kinoshita, Phys. Rev **D57**, 465 (1998).
8. C. Timmermans, Talk at ICHEP98 (Vancouver), see <http://ichep98.triumf.ca/info/sessions/list.asp>.
9. F. A. Paschos and L. Wolfenstein, Phys. Rev. **D7**, 91 (1973).
10. T. Bolton, Talk at ICHEP98 (Vancouver), *loc. cit.*, see also K. S. McFarland *et al.* (NuTeV), Moriond 98, hep-ex/9806013.
11. S. Jadach *et al.*, Proc. ICHEP96 (Warsaw), ed. Z. Ajduk and A. K. Wroblewski (World Sci., 1997) pp 1072-1076, E. Milgiori, *ibid.*, pp 1077-1081.
12. L. Arnaudon *et al.*, CERN SL/94-7 (BI) and other sources can be found at <http://www.cern.ch/LEPECAL/reports/reports.html>.

13. LEP ElectroWeak Working Group, see <http://www.cern.ch/LEPEWWG/>.
Internal note 98-01 was used for the lectures, and plots and numbers used here were current for Vancouver; these have been updated on the web for Vancouver proceedings.
14. P. C. Rowson, Proc. Radiative Corrections, Gatlinburg 1994, ed. B. F. L. Ward (World Sci., 1995) pp 121-137.
15. K. Baird, Talk at ICHEP98 (Vancouver), *loc. cit.*
16. Partical Data Group, C. Caso *et al.*, Eur. Phys. Jour. **C3** (1998) pp 90-102, see <http://pdg.lbl.gov/pdg.html>.
17. S. D. Drell and T. M. Yan, Phys. Rev. Lett. **25**, 316 (1970).
18. C. Balazs *et al.*, Phys. Lett. **B355**, 548 (1995).
19. F. Abe *et al.* (CDF), subm. Phys Rev. Lett., FERMILAB-PUB-98/256-E, hep-ex/9809001, and the references therein.
20. A. Gordon *et al.* (CDF), Proc. Moriond Electroweak (1997), ed. J. Tran Thanh Van, p109.
21. B. Abbott *et al.* (DØ), Phys. Rev. **D58**, 012002 (1998).
22. D. Glenzinski, Talk at Moriond 98 (QCD), hep-ex/9805020.
23. J. Z. Bai *et al.* (BES), Phys. Rev. **D53**, 20 (1996).
24. S. Catani *et al.*, Phys. Lett. **B263**, 491 (1991).
25. S. Bethke *et al.*, Nucl. Phys. **B370**, 310 (1992).
26. ALEPH preprint 98-020 CONF 98-011, source of the figures, is updated to H. Przysieniak, Talk at ICHEP98 (Vancouver), ALEPH 98-058 CONF 98-030, see <http://alephwww.cern.ch/WWW/>.
27. DELPHI preprint 98-85 CONF 153, see <http://delphiwww.cern.ch:8002/vancouver/>, paper 341(WW).
28. F. Abe *et al.* (CDF), Phys. Rev. Letters **80**, 2767 (1998).
29. B. Abbott *et al.* (DØ), Phys. Rev. **D58**, 052001 (1998).
30. R. Partridge, Talk at ICHEP98 (Vancouver), *loc. cit.*
31. D. Amidei *et al.*, Report of the TeV2000 Study Group, FERMILAB-PUB-96-082.
32. M. Acciarri *et al.* (L3), Phys. Lett. **B431**, 437 (1998).
33. R. Peccei, Talk at ICHEP98 (Vancouver), *loc. cit.*
34. F. Abe *et al.* (CDF), Phys. Rev. Lett. **75**, 1017 (1995).
35. B. Abbott *et al.* (DØ), Phys. Rev. **D58**, 031102 (1998).
36. W. Hollik, Talk at ICHEP98 (Vancouver), *loc. cit.*
37. See *eg.* M. Acciarri *et al.* (L3), subm. Phys. Lett. B, CERN-EP/98-072 L3-148.